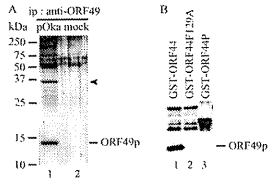

FIG 4 Identification of ORF44p as the binding partner of ORF49p by proteomic analysis and their *in vitro* binding assay. (A) pOka-infected MeWo cells expanded by cell-to-cell spread with full CPE at 2 to 3 days postinfection were lysed with RIPA buffer, and the binding molecules were coimmunoprecipitated with ORF49p using an anti-ORF49 Ab (lane 1). Mock-infected MeWo cells were used as a negative control (lane 2). The immunoprecipitates (ip) were electrophoretically separated and visualized by silver staining. (B) ORF49p expressed in and purified from MeWo cells was incubated with purified GST-ORF44 (*lane 1*), GST-ORF44F129A (lane 2), or GST-ORF44P (lane 3). Bound proteins were electrophoretically separated and visualized by anti-GST Abs (upper panel) and anti-ORF49 Abs (lower panel).

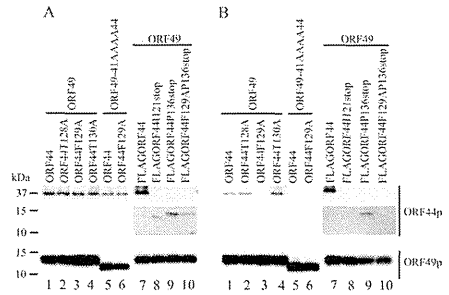

FIG 6 Expression and interaction of ORF44p and ORF49p in cotransfected cells. MeWo cells were cotransfected with CAG/ORF49 (lanes 1 to 4 and 7 to 10) or CAG/ORF49-41AAAA44 (lanes 5 and 6) and CAG/ORF44 (lanes 1 and 5), CAG/ORF44T128A (lane 2), CAG/ORF44F129A (lanes 3 and 6), CAG/ORF44K130A (lane 4), CAG/FLAGORF44 (lane 7), CAG/FLAGORF44I121stop (lane 8), CAG/FLAGORF44P136stop (lane 9), or CAG/FLAGORF44F129AP136stop (lane 10) (A and B). Protein expression was visualized with anti-ORF44p and anti-ORF49p antibodies (A), and proteins immunoprecipitated by anti-ORF49 Ab from cotransfected cells were electrophoretically separated and visualized using anti-ORF44 and anti-ORF49 Abs (B).

between ORF44p and ORF49p were confirmed by immunoblotting with the corresponding Abs and immunoprecipitation with anti-ORF49 Ab followed by immunoblotting with each Ab (Fig. 6A, lane 1, and B, lane 1, respectively). In rpOkaORF49M1LRev-infected MeWo cells, in spite of the broadly diffuse pattern seen for ORF44p, it appeared to accumulate on the TGN with ORF49p (Fig. 7B), as was seen in coexpressing cells (Fig. 5C), and this pattern was also observed in cells infected with rpOka (data not shown). In rpOkaORF49M1L-infected cells, ORF44p was dispersed as in cells expressing ORF44 alone and was not accumulated on the TGN (Fig. 7A), again indicating that the accumulation of ORF44p on the TGN depended on ORF49p and required no other viral factors.

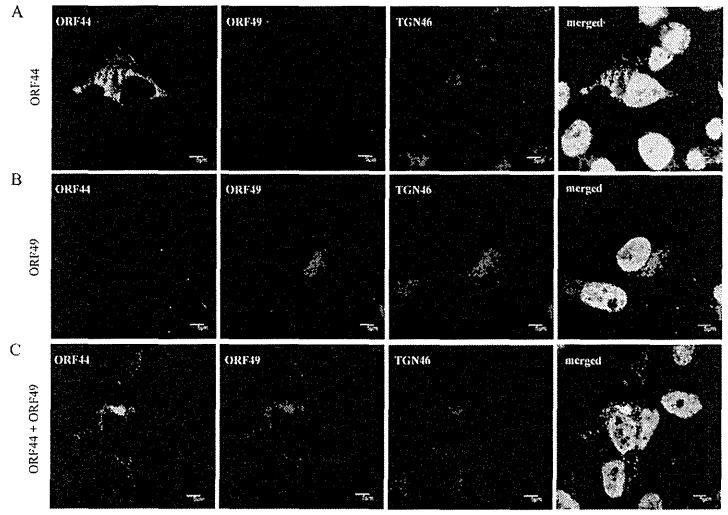

FIG 5 Localization of ORF44p and ORF49p in transiently transfected MeWo cells. MeWo cells were transfected with CAG/ORF44 (A) or CAG/ORF49 (B) or cotransfected with CAG/ORF44 and CAG/ORF49 (C). Cells were fixed at 48 h posttransfection and triple labeled for ORF44p (green), ORF49p (red), and TGN46 (blue). Nuclei were stained with Hoechst 33342 (cyan). Scale bars, 5 μm.

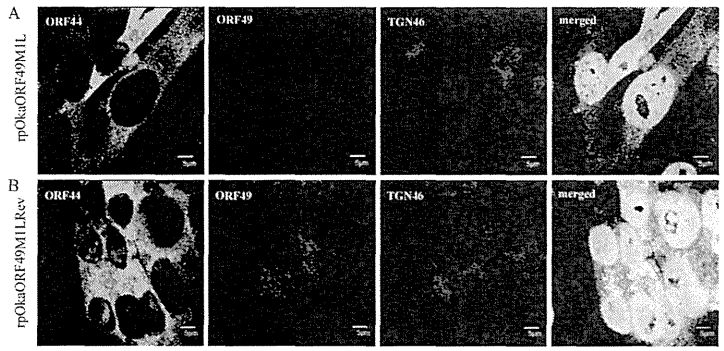

FIG 7 Localization of ORF44p and ORF49p in rpOkaORF49M1L-infected MeWo cells. rpOkaORF49M1L-infected (A) and rpOkaORF49M1LRev-infected (B) MeWo cells were fixed at 48 hpi and triple labeled for ORF44p (green), ORF49p (red), and TGN46 (blue). Nuclei were stained with Hoechst 33342 (cyan). Scale bars, 5 μm.

The phenylalanine at amino acid position 129 of ORF44p functions in the conserved interaction and is essential for VZV infection. In the process of ORF44 cloning, one mutant showed a T-to-C substitution at nt 385, which led to a phenylalanine-to-serine transition at aa 129 (F129S). In cells coexpressing ORF44F129Sp and ORF49p, ORF44F129Sp did not accumulate on the TGN and was not coimmunoprecipitated with ORF49p (data not shown).

To examine whether 129F functions specifically in the conserved interaction in VZV, alanine scanning was performed around 129F (Fig. 1B). ORF44T128Ap, ORF44F129Ap, and ORF44K130Ap showed similar distributions, and none of these mutants localized to the TGN when expressed alone (data not shown), as observed in cells expressing ORF44p alone (Fig. 5A). Coexpression of ORF44T128Ap and ORF44K130Ap with ORF49p (Fig. 8A and C, respectively) resulted in their colocalization with ORF49p at the TGN, as observed in cells coexpressing ORF44p and ORF49p (Fig. 5C). In contrast, ORF44F129Ap was dispersed throughout the cytoplasm and failed to accumulate on the TGN, even when coexpressed with ORF49p (Fig. 8B). The levels of expression of ORF44T128Ap, ORF44F129Ap, and ORF44K130Ap were almost equal (Fig. 6A, lanes 2, 3, and 4, respectively), and ORF44T128Ap and ORF44K130Ap were coimmunoprecipitated with ORF49p (Fig. 6B, lanes 2 and 4, respectively), whereas ORF44F129Ap was not coimmunoprecipitated with ORF49p (Fig. 6B, lane 3).

The results for F129S and F129A suggest that the binding site for ORF49p might reside in an N-terminal domain, as was recently reported for the pUL16 of HSV-1 (26). Therefore, stop codons were inserted at positions to either side of codon 129F (i.e., at I121stop and P136stop). In addition, a construct containing both the F129A and P136stop mutations was made (Fig. 1B). All three mutants were expressed at their predicted size (Fig. 6A, lanes 8, 9, and 10), and only the ORF44P136stop protein was coimmunoprecipitated with ORF49p (Fig. 6B, lane 9), whereas the ORF44I121stop and ORF44F129AP136stop proteins were not (Fig. 6B, lanes 8 and 10, respectively). Consistent with this, only the ORF44P136stop protein accumulated on the TGN with ORF49p (Fig. 8E), and the other two mutants did not (Fig. 8D and F), despite the diffused cytoplasmic localization of all mutants if expressed alone (data not shown). These results show that the binding site for ORF49p resides in the first third of ORF44p and that 129F plays a critical role in binding, either directly or indirectly. Furthermore, in GST-pulldown assays using GST-ORF44 (corresponding to aa 2 to 363), GST-ORF44F129A (aa 2 to 363 with F129A mutation), and GST-ORF44P (aa 180 to 363), only GST-ORF44 pulled down ORF49p expressed in and purified from MeWo cells (Fig. 4B), suggesting that there may not be a binding site within the C-terminal half of ORF44p; however, other C-terminal constructs have not been tested in this or other assays.

To analyze the impact of the 129F mutation in the context of infection, pOka-BACORF44T128A, pOka-BACORF44F129A, pOka-BACORF44K130A, and the revertant BAC for pOka-BACORF44F129A, pOka-BACORF44F129ARev, were generated (Fig. 1B). With the exception of the ORF44F129A mutant, the reconstitution of each virus with a mutation around 129F and of the revertant virus for the F129A mutant was successful, and all of the reconstituted viruses showed similar growth to rpOka (data not shown), suggesting that 129F of ORF44p may play a central role in the function of ORF44p in VZV infection, which occurs through its interaction with ORF49p.

The carboxyl-terminal half of the acidic cluster of ORF49p is required for the conserved interaction with ORF44p. To map the binding domain of ORF49p for ORF44p using the accumulation of ORF44p as an indicator of the interaction, we generated a series of carboxyl-terminal-truncated mutants of ORF49p (Fig. 1C). The coexpression of ORF44p and ORF49N48p or ORF49N44p resulted in the accumulation of ORF44p at the juxtanuclear region with TGN46 and the mutant ORF49p (Fig. 9A and B). In contrast, ORF44p never colocalized with ORF49N40p (Fig. 9C) and was dispersed in the cytoplasm, as when it was expressed alone (Fig. 5A). These results suggested that the ORF44p-binding domain in ORF49p may be located between the aspartate at aa 41 and glutamate at aa 44, which is in the carboxyl-terminal half of the conserved acidic cluster (Fig. 1C) in the ORF49 homologs.

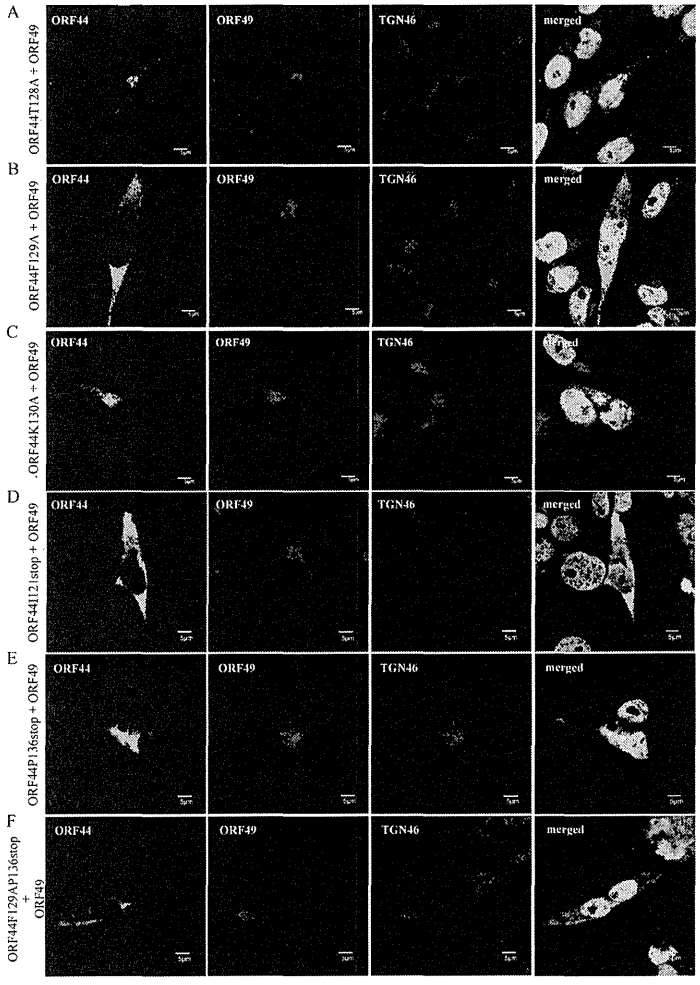

FIG 8 Localization and accumulation of ORF44 mutant proteins in MeWo cells expressing ORF49p. MeWo cells were cotransfected with CAG/ORF49 and CAG/ORF44T128A (A), CAG/ORF44F129A (B), CAG/ORF44K130A (C), CAG/FLAGORF44I121stop (D), CAG/FLAGORF44P136stop (E), or CAG/FLAGORF44F129AP136stop (F). *Cells were fixed at 48 h posttransfection and triple labeled for ORF44 (green), ORF49 (red), and TGN46 (blue). Nuclei were* stained with Hoechst 33342 (cyan). Scale bars, 5 μm.

To confirm the specificity of the ORF44p and ORF49p interaction while avoiding (although not excluding) nonspecific effects on the function of ORF49p resulting from the destruction of the ORF49p backbone, the four residues (41DFDE44) identified as the candidate ORF44p-binding motif were replaced by alanine, resulting in ORF49-41AAAA44p (Fig. 1C). As shown in Fig. 9D, ORF49-41AAAA44p targeted the TGN, similar to ORF49p (Fig. 5B), but it was unable to accumulate ORF44p on the TGN (Fig. 9E).

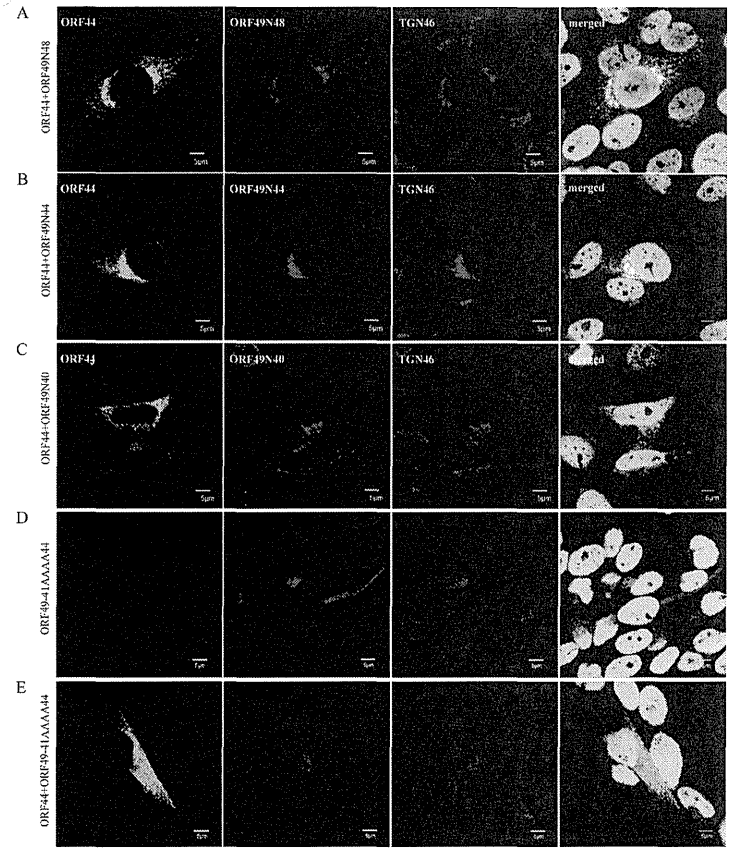

FIG 9 Localization and accumulation of ORF44p in MeWo cells expressing ORF49 mutant proteins. MeWo cells were cotransfected with CAG/ORF44 and CAG/ORF49N48 (A), CAG/ORF49N44 (B), CAG/ORF49N40 (C), or CAG/ORF49-41AAAA44 (E), or transfected with CAG/ORF49-41AAAA44 alone (D). Cells were fixed at 48 h posttransfection and triple labeled for ORF44 (green), ORF49 (red), and TGN46 (blue). Nuclei were stained with Hoechst 33342 (cyan). Scale bars, 5 μm.

Furthermore, ORF49-41AAAA44p did not form a complex with ORF44p or ORF44F129Ap (Fig. 6B, lane 5 or 6) despite the efficient coexpression of all proteins (Fig. 6A, lanes 5 and 6).

The carboxyl-terminal half of the acidic cluster of ORF49p plays a central role in the function of ORF49p during infection. rpOkaORF49-41AAAA44 showed almost the same phenotype as rpOkaORF49M1L, including the loss of the interaction with ORF44p (Fig. 2E, lane 1), the dispersed localization of ORF44p without accumulation on the TGN (Fig. 10A), impaired growth as assessed by plaque size and infectious-center assays (Fig. 11A and B, respectively), and reduced production of infectious progeny virus (to 3 to 10% of the wild-type level [Table 2]), excluding the apparent ORF49-41AAAA44p expression (Fig. 2D, lane 1, and Fig. 10A). These defects were completely rescued by revertant virus infection (Fig. 2D and E, lanes 2, Fig. 10B, and Fig. 11A and B) or by exogenous ORF49p in MeWoORF49 cells (Fig. 11A and B and Table 2). The expression of ORF49-41AAAA44p was detected as a faint and faster-migrating band than that of ORF49p in the revertant virus infection, but an equal amount of ORF44p was detected in both viruses with gH and ORF61p (Fig. 2D, lanes 1 and 2). Furthermore, whereas the interaction between ORF49-41AAAA44p and ORF44p was not detected at all (Fig. 2E, lane 1),

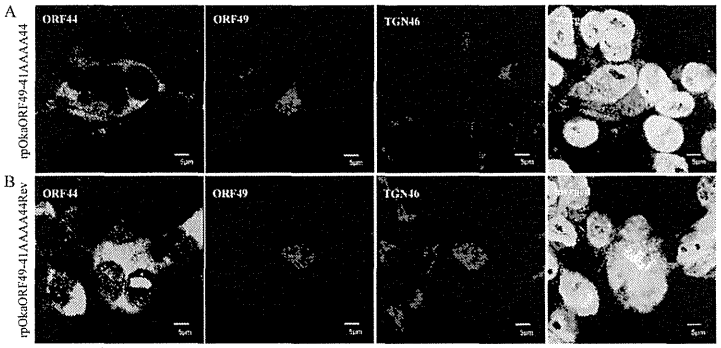

FIG 10 *Localization of ORF44p and ORF49p in rpOkaORF49-41AAAA44-infected MeWo cells.* rpOkaORF49-41AAAA44-infected MeWo cells (A) and rpOkaORF49-41AAAA44Rev-infected MeWo cells (B) were fixed at 48 hpi and triple labeled for ORF44p (green), ORF49p (red), and TGN46 (blue). Nuclei were stained with Hoechst 33342 (cyan). Scale bars, 5 μm.

ORF44p was incorporated into the rpOkaORF49-41AAAA44 particles in the absence or presence of exogenous ORF49p (Fig. 2F, lane 1 or 2), which was also the case in rpOkaORF49M1L infection (Fig. 2D and F).

Taken together, our results indicated that ORF49p functions in the efficient production of progeny viruses required for VZV infection through its interaction with the essential protein ORF44p.

DISCUSSION

In VZV, ORF49 encodes a nonessential tegument protein that is one of the cell-tropic factors in cell culture (6). In human fetal lung fibroblast MRC-5 cells, the growth of ORF49-defective virus is identical to that of its parental virus, whereas in the human melanoma MeWo cell line, it shows reduced growth; however, the cell tropism of VZV for these two most permissive cell lines has not been studied. In the previous study, we showed that it is a cell-tropic factor, although the step(s) at which ORF49 functions, including the entry, host gene modulation, viral gene expression, viral particle assembly, or egress, remained unclear. Nevertheless, we showed that it may play an important role in the production of a complete virion (6).

VZV is highly cell associated *in vitro*, producing extremely small amounts of infectious virus even when isolated intracellularly (in a particle-to-PFU ratio that varies from approximately 40,000 to 1,000,000) (39, 40), and the particles detected by electron microscopy (EM) analysis appear to be degraded, even in cells infected by the wild-type virus (41–43). The low infectivity and the presence of few or no infectious particles in the cell culture

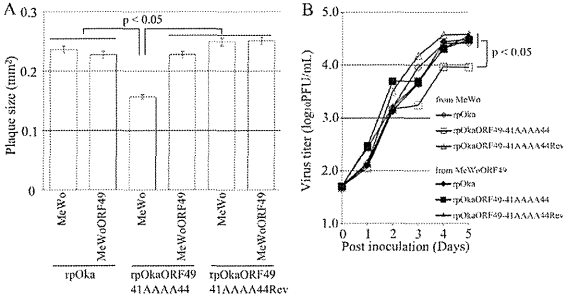

FIG 11 Growth properties of ORF49-41AAAA44 mutant virus in MeWo and MeWoORF49 cells. (A) Comparison of plaque sizes among recombinant viruses. MeWo cells or MeWoORF49 cells were infected with rpOka, rpOkaORF49-41AAAA44, or rpOkaORF49-41AAAA44Rev (50 PFU/well) and cultured for 7 days. Infected cells were stained with an anti-gE Ab, and the plaques were traced and measured by ImageJ software. Plaque size is shown with the standard error of the mean. Statistical significance was determined by Student's *t* test. (B) Growth kinetics of recombinant viruses on MeWo cells and MeWoORF49 cells. MeWo cells or MeWoORF49 cells were infected with rpOka, rpOkaORF49-41AAAA44, or rpOkaORF49-41AAAA44Rev (50 PFU/well), harvested at the indicated times, serially diluted, added to newly prepared MeWo cells, and cultured for 5 days. The plaques were stained with an anti-gE Ab and counted. Each point represents the mean titer for two wells of one experiment. Two experiments were performed independently. Statistical significance was determined by Student's *t* test.

supernatant in VZV have made it difficult to construct a *trans*-complementation system. In such a system, the target viral gene is expressed on permissive cells on which the target gene-deleted virus is only capable of efficient replication similar to the wild-type virus infection on the parental cells. The infection of parental cells by the target gene-deleted virus isolated from cells expressing the target gene enables analysis of its function. This method is useful to confirm that the deletion phenotype is not caused by undesired mutations, which can also be determined by generating the revertant virus to repair the mutated gene within the viral genome. In addition, it can also be used to identify the target gene function, which cannot be determined by simply generating the mutant and revertant viruses and has been used widely in the mutagenic analysis of other herpesviruses, especially in the analysis of structural proteins. However, to the best of our knowledge, this system has been used successfully to analyze gene function in only one report (44) and to confirm that the deletion phenotype is independent of undesired mutation in two reports (45, 46) in VZV research.

In the present study, we established a *trans*-complementation system for ORF49. The ORF49 *trans*-complementation system allowed identification of the precise function of ORF49, which could not be determined by generating its defective virus following EM analysis on MeWo cells. In the EM analysis, no significant differences between the wild-type and ORF49-defective viruses were detected with regard to the intracellular and cell surface viral particle counts or morphology (T. Sadaoka and Y. Mori, unpublished observation), possibly leading to their obvious difference in infectivity, which was reduced by 10-fold or higher in the defective virus. Additionally, in both viruses, the infected cells or viral particles isolated from the same quantity of infected cells contained almost the same amount of viral proteins. The *trans*-complementation system in combination with the results of other analyses described above indicated that ORF49 functions in the production of efficient infectious viruses. The results of EM analysis and immunoblotting suggested that the ORF49 defect did not cause the reduction of viral protein synthesis and viral particle assembly and egress. The cell-free virus titration and plaque formation analyses using the *trans*-complementation system showed that the ORF49p released from the virion into the cells during the entry step was not functional, but *de novo* ORF49p synthesized during lytic replication functioned in the production of efficient infectious virus required for cell-free and cell-to-cell viral transmission modes. However, how the deletion of ORF49 impaired infectivity remained unclear.

To gain further insight into the function of ORF49 during VZV infection, we confirmed ORF44p as its binding partner, as reported in other herpesviruses (12–15), and examined the conserved interaction between these proteins by analyzing their binding properties. We identified 129F in ORF44p as being essential for accumulation on the TGN through the interaction with ORF49p: whether it functions in the binding directly or indirectly is unknown. Simultaneously, 41DFDE44 of the carboxyl-terminal half of the acidic cluster within ORF49p was identified as the binding motif for ORF44p. Among these critical amino acids of ORF44p and ORF49p, each phenylalanine seems to function in the binding. As the phenylalanine is an aromatic and hydrophobic amino acid, it prefers to be buried in protein hydrophobic cores. However, 129F of ORF44p is surrounded by polar amino acid 128T and charged amino acid 130K and 42F of ORF49p by charged amino acids 41D, 43D, and 44E, and there is possibility that these two phenylalanines are exposed at the protein surface. The phenylalanine side chain is fairly nonreactive and is thus rarely directly involved in protein function, although it can play a role in substrate recognition. In particular, hydrophobic amino acids can be involved in binding/recognition of hydrophobic ligands, and the aromatic side chain can also be involved in interactions with other aromatic side chains via stacking interactions (47). In coexpression of ORF44 and ORF49, ORF49F42A mutation alone disrupted the interaction and failed to accumulate ORF44p on the TGN, as seen in ORF49-41AAAA44 mutation, while individual ORF49D41A, -D43A, or -E44A mutation had no effect on them (T. Sadaoka and Y. Mori, unpublished observation). On the other hand, ORF44F129A showed an impaired phenotype in terms of their interaction and its accumulation on the TGN, and neither ORF44T128A nor K130A mutation had any effect on them. However, in the context of infection, ORF49F42A alone could not abrogate the interaction and had no effect on virus growth (T. Sadaoka and Y. Mori, unpublished observation) different from that of ORF49-41AAAA44 mutation (discussed below), while only ORF44F129A was truly lethal for infectious virus production/reconstitution, and again ORF44T128A and ORF44K130A had no effect. These findings may prompt us to conclude that the core machinery of the binding is the noncovalent attractive force between two aromatic rings of phenylalanine and that the additional binding force via charged amino acids around 42F of ORF49p is required in the context of infection; however, there is another possibility—that the ORF44F129A mutation just disrupts the protein structure itself, leading to the loss of interaction. As mentioned above, phenylalanine prefers to be buried in protein hydrophobic cores, and the interaction among the aromatic residues is also important in the protein folding and the structural stabilization of protein (48, 49). Our results about the interaction property revealed that the binding domain within ORF44p is located at the first 136 residues and 129F is essentially involved in the binding, but could not be determined as the precise binding domain, and at the same time, there was no apparent degradation or lower expression of ORF44F129Ap in comparison with ORF44p in both prokaryotic expression and eukaryotic expression systems. To address these issues, further analyses by making an N-terminal truncation for refining the interaction domain and another 129F substitution with tyrosine, which differs only in that it contains a hydroxyl group in place of the ortho hydrogen on the benzene ring, for more preferable substitution to maintain structural stability will be helpful and ongoing.

Assessment of the function of ORF44 in the context of infection did not reveal new findings, with the exception of the F129A mutant, which showed the same phenotype as the deletion mutant. The ORF44 deletion and F129A mutation were lethal for progeny virus production/reconstitution in MeWo and MRC-5 cells; however, an effective *trans*-complementation system for ORF44 as for ORF49 was not successfully established, and at what step(s) in the lytic infection ORF44 essentially functions remained unclear. To find the nonessential but important functions of ORF44 in the context of infection, we turned back to analyzing the ORF49 function by generating ORF49-41AAAA44 virus, in which ORF49p specifically lost the interaction with ORF44p, following comparison of the phenotype between ORF49-defective virus and ORF49-41AAAA44 virus. The rpOkaORF49-41AAAA44 virus showed the same phenotype as the rpOkaORF49M1L virus, indicating that the function of ORF49p in the efficient production of

progeny viruses was completely dependent on the interaction with ORF44p at 41DFDE44. These results suggest that ORF44p is fully functional only in the presence of ORF49p and vice versa and has essential functions during infection, which are independent of the interaction with ORF49p or redundantly supported by other viral factors in the absence of ORF49p.

In the absence of the interaction with ORF49p during infection, ORF44p was detected throughout the cytoplasm and rarely colocalized with the TGN (or with a reorganized organ containing TGN-derived membranes known to be induced by viral infection, although it has not been found in VZV infection), the recognized site of viral assembly; however, incorporation of ORF44p into viral particles was comparable to that observed in wild-type virus infection. These results indicate that ORF44p was not directly incorporated into the particles through the TGN via its interaction with ORF49p, at least in the absence of ORF49p. In HSV-1, the amount of pUL16 packaged into the viral particles was severely reduced in the absence of pUL11 (50), but there are some other interaction partners that potentially function in incorporating pUL16 into the viral particles (i.e., pUL21 and glycoprotein E) (51, 52). In VZV, by global screening using the yeast two-hybrid system, some candidates for ORF44p binding partner have been reported (28, 29), but in our observations, none of these viral proteins other than ORF49p could accumulate ORF44p on the TGN; one viral protein could alter the localization of ORF44p into the nucleus; however, whether it functions in the incorporation of ORF44p into the viral particles remained unclear (T. Sadaoka and Y. Mori, unpublished observation). Anyway, additional ORF44p binding partners active during either the wild-type virus or ORF49-defective virus infection remain to be identified so far, and the complexity of the herpesvirus protein-protein network requires a solid approach to elucidate the essential roles of ORF44 during viral infection further through the interactions with other viral proteins.

In summary, in the present study, we established a *trans*-complementation system for ORF49 and identified ORF44p as the binding partner for ORF49p. We showed that (i) ORF49p functions in the efficient production of infectious virus, (ii) no other viral factor is required for binding, (iii) residue 129F of ORF44p is critical not only for binding to ORF49p but also for progeny virus production/reconstitution, (iv) the carboxyl-terminal half of the acidic cluster (41DFDE44) of ORF49p is the binding motif for ORF44p, and (v) the efficient production of infectious progeny virus by ORF49p is dependent on its interaction with ORF44p. Further analyses of the role of ORF44 mediated by its interaction with ORF49 or other as yet unidentified viral proteins may shed light on the conserved infection mechanisms of the *Herpesvirinae* and those unique to VZV.

ACKNOWLEDGMENTS

We thank Eiko Moriishi (National Institute of Biomedical Innovation, Osaka, Japan) for technical assistance, Panayiotis A. Ioannou (Cell and Gene Therapy Research Group, The Murdoch Children's Research Institute, The University of Melbourne, Royal Children's Hospital, Melbourne, Australia) for providing pGETrec, Wilfried Wackernagel (Genetics, Department of Biology and Environmental Sciences, Universität Oldenburg, Germany) for pCP20, Jun-ichi Miyazaki (Division of Stem Cell Regulation Research, Osaka University Graduate School of Medicine, Japan) for pCAGGS, Masaru Okabe (Department of Experimental Genome Research, Genome Information Research Center, Osaka University, Japan) for pCX-Cre, and Ulrich H. Koszinowski (Max von Pettenkofer Institut fur Virologie, Ludwig-Maximilians-Universität München, Germany) for pHA2 and pST76A-SR.

This study was supported in part by a Grant-in-Aid for Scientific Research on Priority Areas (21022031 to Y.M.) from the Ministry of Education, Culture, Sports, Science, and Technology (MEXT) of Japan, a Grant-in-Aid for Scientific Research (B) (20390138 to Y.M.), a Grant-in-Aid for Young Scientists (B) (20790363 and 22790432 to T.S.), a Grant-in-Aid for Scientific Research (C) (24590551 to T.S.) from the Japan Society for the Promotion of Science (JSPS), and a grant from the Uehara Memorial Foundation (to T.S.).

REFERENCES

1. **Moffat J, Ku CC, Zerboni L, Sommer M, Arvin A.** 2007. VZV: pathogenesis and the disease consequences of primary infection, p 675–688. *In* Arvin A, Campadelli-Fiume G, Mocarski E, Moore PS, Roizman B, Whitley R, Yamanishi K (ed), Human herpesviruses: biology, therapy, and immunoprophylaxis. Cambridge University Press, Cambridge, United Kingdom.
2. **Baines JD, Pellett PE.** 2007. *Genetic comparison of human alphaherpesvirus genomes*, p 61–69. *In* Arvin A, Campadelli-Fiume G, Mocarski E, Moore PS, Roizman B, Whitley R, Yamanishi K (ed), Human herpesviruses: biology, therapy, and immunoprophylaxis. Cambridge University Press, Cambridge, United Kingdom.
3. **Davison AJ, Scott JE.** 1986. The complete DNA sequence of varicella-zoster virus. J. Gen. Virol. 67:1759–1816. http://dx.doi.org/10.1099/0022-1317-67-9-1759.
4. **Davison AJ.** 2007. Comparative analysis of the genomes, p 10–26. *In* Arvin A, Campadelli-Fiume G, Mocarski E, Moore PS, Roizman B, Whitley R, Yamanishi K (ed), Human herpesviruses: biology, therapy, and immunoprophylaxis. Cambridge University Press, Cambridge, United Kingdom.
5. **Zhang Z, Selariu A, Warden C, Huang G, Huang Y, Zaccheus O, Cheng T, Xia N, Zhu H.** 2010. Genome-wide mutagenesis reveals that ORF7 is a novel VZV skin-tropic factor. PLoS Pathog. 6:e1000971. http://dx.doi.org/10.1371/journal.ppat.1000971.
6. **Sadaoka T, Yoshii H, Imazawa T, Yamanishi K, Mori Y.** 2007. Deletion in open reading frame 49 of varicella-zoster virus reduces virus growth in human malignant melanoma cells but not in human embryonic fibroblasts. J. Virol. 81:12654–12665. http://dx.doi.org/10.1128/JVI.01183-07.
7. **Baines JD, Jacob RJ, Simmerman L, Roizman B.** 1995. The herpes simplex virus 1 UL11 proteins are associated with cytoplasmic and nuclear membranes and with nuclear bodies of infected cells. J. Virol. 69:825–833.
8. **Britt WJ, Jarvis M, Seo JY, Drummond D, Nelson J.** 2004. Rapid genetic engineering of human cytomegalovirus by using a lambda phage linear recombination system: demonstration that pp28 (UL99) is essential for production of infectious virus. J. Virol. 78:539–543. http://dx.doi.org/10.1128/JVI.78.1.539-543.2004.
9. **Silva MC, Yu QC, Enquist L, Shenk T.** 2003. Human cytomegalovirus UL99-encoded pp28 is required for the cytoplasmic envelopment of tegument-associated capsids. J. Virol. 77:10594–10605. http://dx.doi.org/10.1128/JVI.77.19.10594-10605.2003.
10. **MacLean CA, Dolan A, Jamieson FE, McGeoch DJ.** 1992. The myristylated virion proteins of herpes simplex virus type 1: investigation of their role in the virus life cycle. J. Gen. Virol. 73:539–547. http://dx.doi.org/10.1099/0022-1317-73-3-539.
11. **Silva MC, Schroer J, Shenk T.** 2005. Human cytomegalovirus cell-to-cell spread in the absence of an essential assembly protein. Proc. Natl. Acad. Sci. U. S. A. 102:2081–2086. http://dx.doi.org/10.1073/pnas.0409597102.
12. **Loomis JS, Courtney RJ, Wills JW.** 2003. Binding partners for the UL11 tegument protein of herpes simplex virus type 1. J. Virol. 77:11417–11424. http://dx.doi.org/10.1128/JVI.77.21.11417-11424.2003.
13. **Guo H, Wang L, Peng L, Zhou ZH, Deng H.** 2009. Open reading frame 33 of a gammaherpesvirus encodes a tegument protein essential for virion morphogenesis and egress. J. Virol. 83:10582–10595. http://dx.doi.org/10.1128/JVI.00497-09.
14. **Liu Y, Cui Z, Zhang Z, Wei H, Zhou Y, Wang M, Zhang XE.** 2009. The tegument protein UL94 of human cytomegalovirus as a binding partner for tegument protein pp28 identified by intracellular imaging. Virology 388:68–77. http://dx.doi.org/10.1016/j.virol.2009.03.007.
15. **Maninger S, Bosse JB, Lemnitzer F, Pogoda M, Mohr CA, von Einem J, Walther P, Koszinowski UH, Ruzsics Z.** 2011. M94 is essential for the secondary envelopment of murine cytomegalovirus. J. Virol. 85:9254–9267. http://dx.doi.org/10.1128/JVI.00445-11.
16. **Meckes DG, Jr, Wills JW.** 2007. Dynamic interactions of the UL16 tegument protein with the capsid of herpes simplex virus. J. Virol. 81:13028–13036. http://dx.doi.org/10.1128/JVI.01306-07.
17. **Nalwanga D, Rempel S, Roizman B, Baines JD.** 1996. The UL 16 gene product of herpes simplex virus 1 is a virion protein that colocalizes with intranuclear capsid proteins. Virology 226:236–242. http://dx.doi.org/10.1006/viro.1996.9651.
18. **Oshima S, Daikoku T, Shibata S, Yamada H, Goshima F, Nishiyama Y.** 1998. Characterization of the UL16 gene product of herpes simplex virus type 2. Arch. Virol. 143:863–880. http://dx.doi.org/10.1007/s007050050338.
19. **Yeh PC, Meckes DG, Jr, Wills JW.** 2008. Analysis of the interaction between the UL11 and UL16 tegument proteins of herpes simplex virus. J. Virol. 82:10693–10700. http://dx.doi.org/10.1128/JVI.01230-08.
20. **Johnson DC, Baines JD.** 2011. Herpesviruses remodel host membranes for virus egress. Nat. Rev. Microbiol. 9:382–394. http://dx.doi.org/10.1038/nrmicro2559.
21. **Baines JD, Roizman B.** 1991. The open reading frames UL3, UL4, UL10, and UL16 are dispensable for the replication of herpes simplex virus 1 in cell culture. J. Virol. 65:938–944.
22. **Dunn W, Chou C, Li H, Hai R, Patterson D, Stolc V, Zhu H, Liu F.** 2003. Functional profiling of a human cytomegalovirus genome. Proc. Natl. Acad. Sci. U. S. A. 100:14223–14228. http://dx.doi.org/10.1073/pnas.2334032100.
23. **Klupp BG, Bottcher S, Granzow H, Kopp M, Mettenleiter TC.** 2005. Complex formation between the UL16 and UL21 tegument proteins of pseudorabies virus. J. Virol. 79:1510–1522. http://dx.doi.org/10.1128/JVI.79.3.1510-1522.2005.
24. **Phillips SL, Bresnahan WA.** 2012. The human cytomegalovirus (HCMV) tegument protein UL94 is essential for secondary envelopment of HCMV virions. J. Virol. 86:2523–2532. http://dx.doi.org/10.1128/JVI.06548-11.
25. **Yu D, Silva MC, Shenk T.** 2003. Functional map of human cytomegalovirus AD169 defined by global mutational analysis. Proc. Natl. Acad. Sci. U. S. A. 100:12396–12401. http://dx.doi.org/10.1073/pnas.1635160100.
26. **Chadha P, Han J, Starkey JL, Wills JW.** 2012. Regulated interaction of tegument proteins UL16 and UL11 from herpes simplex virus. J. Virol. 86:11886–11898. http://dx.doi.org/10.1128/JVI.01879-12.
27. **Phillips SL, Cygnar D, Thomas A, Bresnahan WA.** 2012. Interaction between the human cytomegalovirus tegument proteins UL94 and UL99 is essential for virus replication. J. Virol. 86:9995–10005. http://dx.doi.org/10.1128/JVI.01078-12.
28. **Stellberger T, Hauser R, Baiker A, Pothineni VR, Haas J, Uetz P.** 2010. Improving the yeast two-hybrid system with permutated fusions proteins: the varicella zoster virus interactome. Proteome Sci. 8:8. http://dx.doi.org/10.1186/1477-5956-8-8.
29. **Uetz P, Dong YA, Zeretzke C, Atzler C, Baiker A, Berger B, Rajagopala SV, Roupelieva M, Rose D, Fossum E, Haas J.** 2006. Herpesviral protein networks and their interaction with the human proteome. Science 311:239–242. http://dx.doi.org/10.1126/science.1116804.
30. **Sadaoka T, Yanagi T, Yamanishi K, Mori Y.** 2010. Characterization of the varicella-zoster virus ORF50 gene, which encodes glycoprotein M. J. Virol. 84:3488–3502. http://dx.doi.org/10.1128/JVI.01838-09.
31. **Niwa H, Yamamura K, Miyazaki J.** 1991. Efficient selection for high-expression transfectants with a novel eukaryotic vector. Gene 108:193–199. http://dx.doi.org/10.1016/0378-1119(91)90434-D.
32. **Sadaoka T, Yamanishi K, Mori Y.** 2006. Human herpesvirus 7 U47 gene products are glycoproteins expressed in virions and associate with glycoprotein H. J. Gen. Virol. 87:501–508. http://dx.doi.org/10.1099/vir.0.81374-0.
33. **Okuno T, Yamanishi K, Shiraki K, Takahashi M.** 1983. Synthesis and processing of glycoproteins of varicella-zoster virus (VZV) as studied with monoclonal antibodies to VZV antigens. Virology 129:357–368. http://dx.doi.org/10.1016/0042-6822(83)90175-7.
34. **Nagaike K, Mori Y, Gomi Y, Yoshii H, Takahashi M, Wagner M, Koszinowski U, Yamanishi K.** 2004. Cloning of the varicella-zoster virus genome as an infectious bacterial artificial chromosome in Escherichia coli. Vaccine 22:4069–4074. http://dx.doi.org/10.1016/j.vaccine.2004.04.062.
35. **Narayanan K, Williamson R, Zhang Y, Stewart AF, Ioannou PA.** 1999. Efficient and precise engineering of a 200 kb beta-globin human/bacterial artificial chromosome in E. coli DH10B using an inducible homologous recombination system. Gene Ther. 6:442–447. http://dx.doi.org/10.1038/sj.gt.3300901.
36. **Cherepanov PP, Wackernagel W.** 1995. Gene disruption in Escherichia coli: TcR and KmR cassettes with the option of Flp-catalyzed excision of the antibiotic-resistance determinant. Gene 158:9–14. http://dx.doi.org/10.1016/0378-1119(95)00193-A.
37. **Hobom U, Brune W, Messerle M, Hahn G, Koszinowski UH.** 2000. Fast screening procedures for random transposon libraries of cloned herpesvirus genomes: mutational analysis of human cytomegalovirus envelope glycoprotein genes. J. Virol. 74:7720–7729. http://dx.doi.org/10.1128/JVI.74.17.7720-7729.2000.
38. **Shevchenko A, Wilm M, Vorm O, Mann M.** 1996. Mass spectrometric sequencing of proteins silver-stained polyacrylamide gels. Anal. Chem. 68:850–858. http://dx.doi.org/10.1021/ac950914h.
39. **Carpenter JE, Henderson EP, Grose C.** 2009. Enumeration of an extremely high particle-to-PFU ratio for varicella-zoster virus. J. Virol. 83:6917–6921. http://dx.doi.org/10.1128/JVI.00081-09.
40. **Shiraki K, Takahashi M.** 1982. Virus particles and glycoprotein excreted from cultured cells infected with varicella-zoster virus (VZV). J. Gen. Virol. 61:271–275. http://dx.doi.org/10.1099/0022-1317-61-2-271.
41. **Gabel CA, Dubey L, Steinberg SP, Sherman D, Gershon MD, Gershon AA.** 1989. Varicella-zoster virus glycoprotein oligosaccharides are phosphorylated during posttranslational maturation. J. Virol. 63:4264–4276.
42. **Gershon AA, Sherman DL, Zhu Z, Gabel CA, Ambron RT, Gershon MD.** 1994. Intracellular transport of newly synthesized varicella-zoster virus: final envelopment in the trans-Golgi network. J. Virol. 68:6372–6390.
43. **Harson R, Grose C.** 1995. Egress of varicella-zoster virus from the melanoma cell: a tropism for the melanocyte. J. Virol. 69:4994–5010.
44. **Ali MA, Li Q, Fischer ER, Cohen JI.** 2009. The insulin degrading enzyme binding domain of varicella-zoster virus (VZV) glycoprotein E is important for cell-to-cell spread and VZV infectivity, while a glycoprotein I binding domain is essential for infection. Virology 386:270–279. http://dx.doi.org/10.1016/j.virol.2009.01.023.
45. **Tischer BK, Kaufer BB, Sommer M, Wussow F, Arvin AM, Osterrieder N.** 2007. A self-excisable infectious bacterial artificial chromosome clone of varicella-zoster virus allows analysis of the essential tegument protein encoded by ORF9. J. Virol. 81:13200–13208. http://dx.doi.org/10.1128/JVI.01148-07.
46. **Yamagishi Y, Sadaoka T, Yoshii H, Somboonthum P, Imazawa T, Nagaike K, Ozono K, Yamanishi K, Mori Y.** 2008. Varicella-zoster virus glycoprotein M homolog is glycosylated, is expressed on the viral envelope, and functions in virus cell-to-cell spread. J. Virol. 82:795–804. http://dx.doi.org/10.1128/JVI.01722-07.
47. **Betts MJ, Russell RB.** 22 May 2003. *Amino acid properties and consequences of substitutions*. Chapter 14. *In* Barnes MR, Gray IC (ed), Bioinformatics for geneticists. Wiley, Chichester, West Sussex, England. http://dx.doi.org/10.1002/0470867302.ch14.
48. **Burley SK, Petsko GA.** 1985. Aromatic-aromatic interaction: a mechanism of protein structure stabilization. Science 229:23–28. http://dx.doi.org/10.1126/science.3892686.
49. **Eidenschink LA, Kier BL, Andersen NH.** 2009. Determinants of fold stabilizing aromatic-aromatic interactions in short peptides. Adv. Exp. Med. Biol. 611:73–74. http://dx.doi.org/10.1007/978-0-387-73657-0_32.
50. **Meckes DG, Jr, Marsh JA, Wills JW.** 2010. Complex mechanisms for the packaging of the UL16 tegument protein into herpes simplex virus. Virology 398:208–213. http://dx.doi.org/10.1016/j.virol.2009.12.004.
51. **Han J, Chadha P, Meckes DG, Jr, Baird NL, Wills JW.** 2011. Interaction and interdependent packaging of tegument protein UL11 and glycoprotein E of herpes simplex virus. J. Virol. 85:9437–9446. http://dx.doi.org/10.1128/JVI.05207-11.
52. **Harper AL, Meckes DG, Jr, Marsh JA, Ward MD, Yeh PC, Baird NL, Wilson CB, Semmes OJ, Wills JW.** 2010. Interaction domains of the UL16 and UL21 tegument proteins of herpes simplex virus. J. Virol. 84:2963–2971. http://dx.doi.org/10.1128/JVI.02015-09.

Microbiology and Immunology

Microbiol Immunol 2014; 58: 119–125
doi: 10.1111/1348-0421.12121

ORIGINAL ARTICLE

MHC class I molecules are incorporated into human herpesvirus-6 viral particles and released into the extracellular environment

Megumi Ota[1], Satoshi Serada[2], Tetsuji Naka[2] and Yasuko Mori[1]

[1]Division of Clinical Virology, Center for Infectious Diseases, Kobe University Graduate School of Medicine, 7-5-1, Kusunoki-cho, Chuo-ku, Kobe 650-0017, Japan and [2]Laboratory of Immune Signal, Division of Biomedical Research, National Institute of Biomedical Innovation, 7-6-8, Saito-Asagi, Ibaraki, Osaka 567-0085, Japan

ABSTRACT

Human herpesvirus-6 (HHV-6), which belongs to the betaherpesvirus subfamily, mainly replicates in T lymphocytes. Here, we show that MHC class I molecules are incorporated into HHV-6 viral particles and released into the extracellular environment. In addition, HHV-6A/B-infected T cells showed reduced surface and intracellular expression of MHC class I molecules. The cellular machinery responsible for molecular transport appears to be modified upon HHV-6 infection, causing MHC class I molecules to be transported to virion assembly sites.

Key words human herpesvirus-6A/B, MHC class I, viral particles.

Human herpesvirus 6 (HHV-6), which belongs to the betaherpesvirus subfamily (1), was first isolated from peripheral blood lymphocytes obtained from patients with lymphoproliferative disorders (2). HHV-6 isolates are classified as HHV-6A and HHV-6B based on genetic and antigenic differences and their cell tropism (2–5). Primary infection with HHV-6B causes exanthem subitum (6). The diseases caused by HHV-6A are so far unknown. HHV-6B mostly infects infants and remains latent in more than 90% of the population (7).

In general, herpesviruses use several strategies to evade host immune responses. For example, viruses may inhibit MHC class I-associated antigen presentation to escape detection by cytotoxic T lymphocytes. Several proteins expressed by herpesviruses block the transport of antigenic peptides from the cytosol to the endoplasmic reticulum (8–11), whereas others retain (12–14) or destroy class I molecules, or deliver them to lysosomes for degradation (15–18). The result is reduced surface expression of MHC class I molecules, enabling the virus to evade host immune surveillance.

HHV-6A, but not HHV-6B, downregulates expression of MHC class I in dendritic cells (19). HHV-6 U21 binds to and diverts MHC class I molecules to an endolysosomal compartment, effectively removing them from the cell surface and providing a possible means of immune escape (20).

Here, we show that expression of MHC class I molecules by infected cells is downregulated with incorporation into HHV-6 viral particles, suggesting a possible mechanism by which the virus escapes host immune surveillance.

MATERIALS AND METHODS

Cells and viruses

CBMCs were prepared as described previously (21). CBMCs were provided by K. Adachi (Minoh Hospital, Minoh, Japan) and H. Yamada (Kobe University Graduate School of Medicine, Kobe, Japan) and purchased from the Cell Bank of the RIKEN BioResource Center, Tsukuba, Japan. Virus stocks were also prepared as described previously (21, 22). HSB-2 and MT-4 cell lines were used in this study (23). HHV-6A (strain GS) and HHV-6B (strain HST) were prepared as previously described (21).

Antibodies

Monoclonal antibody (Mab) OHV-1 (24) and a polyclonal antibody against gB (23, 25) have been described previously. The following other Mabs were purchased: MHC class I (clone: W6/32; Bio Legend, San Diego, CA, USA), CD63 (clone: CLB-gran/12, 435; Sanquin Blood Supply, Amsterdam, the Netherlands), and α-tubulin (clone: B-5-1-2; Sigma, St Louis, MO, USA). The following secondary antibodies were used: Alexa Fluor 488- or 594-conjugated F(ab′)2 fragment of goat anti-mouse or rabbit immunoglobulin G (IgG) (Invitrogen, Tokyo, Japan) and anti-mouse IgG, horseradish peroxidase-linked whole antibody (from sheep) (GE Healthcare, Piscataway, NJ, USA).

Virion and exosome isolation

Virions and exosomes were purified as previously described (23, 26). The collected fractions were used for western blotting, electron microscopy or liquid chromatography-tandem mass spectrometry (LC-MS/MS).

Liquid chromatography-tandem mass spectrometry

The fractions described above were analyzed by LC-MS/MS. Proteins were diluted tenfold with 9.8 M urea. The solutions were adjusted to pH 8.5, reduced with 13 mM dithiothreitol at 37°C for 1.5 hr and alkylated with 27 mM iodoacetamide in the dark for 1 hr. The protein mixtures were further diluted with 100 mM triethylammonium bicarbonate (pH 8.5) to reduce urea to 1 M, and digested with 4 μL of 1 mg/mL trypsin–tosyl phenylalanyl chloromethyl ketone solution. Samples were digested overnight at 37°C. Following digestion, lysates were acidified by adding 10% trifluoroacetic acid. The samples were desalted using peptide cleanup C18 spin tubes (Agilent Technologies, Santa Clara, CA, USA) and vacuum-dried. NanoLC-MS/MS analyses were performed on an LTQ-Orbitrap XL mass spectrometer (Thermo Fisher Scientific, Waltham, MA, USA) as described previously (27), while spray voltage was changed to 1800 V. Peptides and proteins were identified by automated database searches using Proteome Discoverer v.1.1 (Thermo Fisher Scientific) against all entries of the Swiss Prot protein database (version 3.26) with a precursor mass tolerance of 10 p.p.m., a fragment ion mass tolerance of 0.8 Da, and strict trypsin specificity, allowing for up to two missed cleavages. Cysteine carbamidomethylation was set as a fixed modification, and methionine oxidation was allowed as a variable modification.

Western blotting

Western blotting was performed as described previously (28, 29).

Electron microscopy

Electron microscopy was performed as described previously (30).

Briefly, the virion-containing pellets were resuspended in 2% (w/v) paraformaldehyde solution buffered with 0.1 M phosphate (pH 7.2). Next, 5 μL of the resuspended pellet was loaded onto formvar–carbon-coated grids to adsorb the virions. Immunostaining was then performed. The virions were incubated with mouse anti-gB, anti-MHC class I or anti-CD63 antibody for 1 hr at room temperature, followed by goat anti-mouse IgG conjugated to 10 nm colloidal gold particles (GE Healthcare) for a further 1 hr at room temperature. After immunolabeling, the samples were washed in distilled water, stained for 5 min with uranyl oxalate, pH 7.0, washed again, embedded in a mixture of 1.8% methylcellulose and 0.4% uranyl acetate, pH 4.0, at 4°C, air-dried, and observed under a Hitachi H-7100 electron microscope (Hitachi, Tokyo, Japan). For the control experiments, samples were incubated with the secondary antibody alone.

Flow cytometry

MT-4 cells were infected with HHV-6B. At 72 hr post-infection, the cells were fixed with 4% (w/v) paraformaldehyde at room temperature for 15 min and incubated with anti-MHC class I Mab at 37°C for 1 hr. The cells were then stained with an appropriate secondary antibody at 37°C for 30 min. For the control experiments, samples were incubated with the secondary antibody alone. Stained cells were analyzed using a flow cytometer (ec800; Sony, Tokyo, Japan).

Immunofluorescence assay

Immunofluorescence assay was performed as described previously (28). Briefly, MT-4 cells were infected with HHV-6B. At 72 hr post-infection, the cells were fixed with cold acetone–methanol (7:3) and incubated at 37°C

Correspondence
Yasuko Mori, Division of Clinical Virology, Center for Infectious Diseases, Kobe University Graduate School of Medicine, 7-5-1, Kusunoki-cho, Chuo-ku, Kobe 650-0017, Japan.
Tel: +81 78 382 6878; fax: +81 78 382 6879; email: ymori@med.kobe-u.ac.jp

Received 17 October 2013; revised 22 November 2013; accepted 6 December 2013.

List of Abbreviations: CBMC, umbilical cord blood mononuclear cell; LC-MS/MS, liquid chromatography-tandem mass spectrometry; HHV-6A, human herpesvirus-6A; HHV-6B, human herpesvirus-6B; MVB, multivesicular body; TGN, *trans*-Golgi network.

for 1 hr with an anti-HHV-6 gB rabbit antibody or an anti-MHC class I Mab. After washing for 10 min with PBS containing 0.02% Tween-20, the cells were incubated with an appropriate secondary antibody at 37°C for 30 min, followed by Hoechst33342 at 37°C for 40 min. After washing as described above, signals were detected by a confocal laser-scanning microscope (Olympus FluoView FV1000; Olympus, Tokyo, Japan).

RESULTS

Virion and exosome isolation

Extracellular viral particles containing exosomes were purified from the culture supernatant of HHV-6A (strain GS)-infected HSB-2 or HHV-6B (strain HST)-infected MT-4 cells. The particle-containing fractions were confirmed by western blotting with an anti-gB antibody (23, 25). Next, the particle-containing fractions were analyzed by LC-MS/MS (27), which detected many cellular proteins (unpublished data). Of the host proteins detected, our analyses focused on MHC class I molecules.

Virion- or exosome-associated fractions contain MHC class I molecules

To verify expression of MHC class I within viral particles, the proteins in fractions 3–10 were separated by SDS–PAGE and analyzed by western blotting with anti-gB rabbit, anti-MHC class I or anti-CD63 antibodies. As shown in Figure 1, gB protein was detected in fractions 5–6 whereas MHC class I was detected primarily in fractions 6–8. We have previously reported that the MVB marker, CD63, is incorporated into virions and exosomes (23); therefore, expression of CD63 was also examined. As expected, CD63 was detected in fractions 5–10 (Fig. 1c). To confirm expression of MHC class I within both virions and exosomes, negative staining of fractions 6 and 7 were performed, followed by electron microscopy (30). Fraction 6 contained mainly viral particles of diameter approximately 200 nm. Both MHC class I (Fig. 1e) and gB protein (Fig. 1d) were present in these particles. Fraction 7 contained mainly exosomes of diameter approximately 50–100 nm (Fig. 1f). These exosomes contained MHC class I, which confirmed the results of the western blotting experiments. Taken together, these results indicate that MHC class I molecules are present in exosomes and virions released from HHV-6B-infected cells.

Downregulated expression of MHC class I molecules on the surface of HHV-6B-infected cells

Downregulation of MHC class I occurs in many different virus-infected cells (31–37). Because MHC class I molecules were incorporated into virions, HHV-6-infected MT-4 cells might show an apparent down-regulation in cell surface expression. To confirm this, HHV-6B- or mock-infected cells harvested 72 hr post-infection were fixed and then stained with an anti-MHC class I antibody. Surface expression of MHC class I was then analyzed by flow cytometry. As expected, HHV-6B-infected cells showed downregulated cell surface expression of MHC class I when compared with mock-infected cells (Fig. 2a). This reduced expression was confirmed by western blot analysis (Fig. 2b), indicating that expression of MHC class I molecules within HHV-6-infected cells (not just expression on the cell surface) was also downregulated. Next, the localization of MHC class I molecules in these cells was assessed after they had been fixed and co-stained with anti-MHC class I and gB antibodies. MHC class I in infected cells was localized mainly within intracellular compartments, and colocalized with the envelope glycoprotein gB during the later stages of infection; however, MHC class I was mainly localized to the plasma membrane in mock-infected cells (Fig. 2c).

DISCUSSION

Here, we used mass spectrometry-based proteomics analysis to show that MHC class I molecules are incorporated into HHV-6 viral particles. Downregulation of MHC class I molecules in virus-infected cells is an important mechanism by which viruses evade immune surveillance (31–37). We showed that downregulation of MHC class I molecules occurs in T cells infected by HHV-6. MHC class I molecules are incorporated into viral particles and exosomes and then released into the extracellular environment, suggesting a possible strategy for escaping host immune responses. In addition, MHC class I molecules incorporated into virions and exosomes may assist viral entry. Further studies are needed to address this question.

We have previously reported that immature HHV-6 particles bud into TGN or TGN-derived vesicles (which are produced in HHV-6B-infected cells), that vesicles containing mature virions become MVBs, and that virions and exosomes are released into the extracellular environment via an exosomal secretary pathway (23). It is possible that MHC class I molecules are transported into the TGN-derived membranes from which the virions bud and then incorporated into virions within infected cells without being recycled (Fig. 3).

Within infected cells, MHC class I molecules colocalized with the gB protein in the cytoplasm indicating that, like viral glycoproteins, they are sorted into vesicles. The reduction in the total (both cell surface and

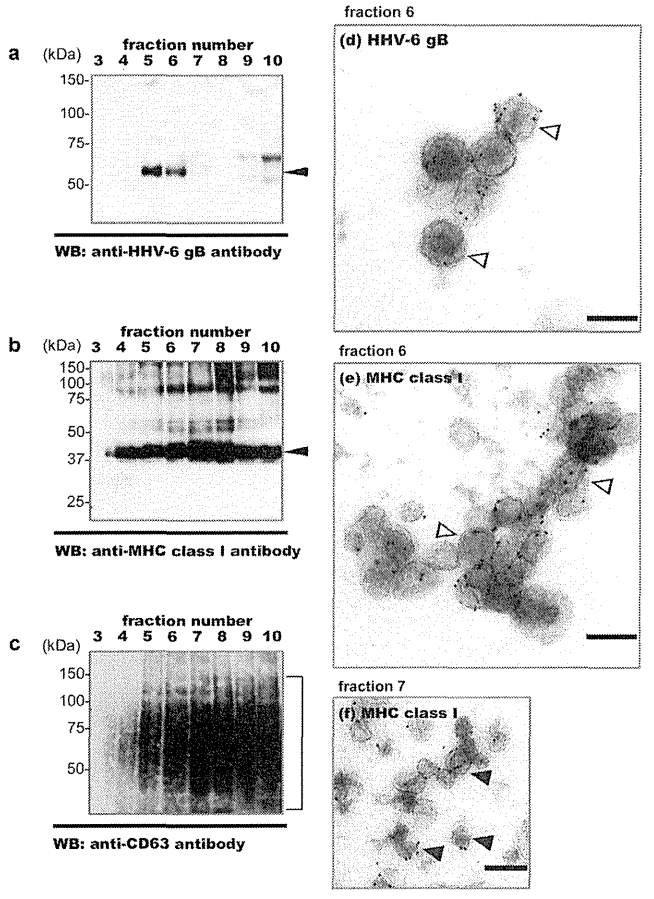

Fig. 1. MHC class I molecules are incorporated into virions and exosomes and released from HHV-6B-infected cells. Virions and exosomes were collected from the culture medium of HHV-6B-infected cells by sucrose density gradient centrifugation and examined by (a–c) western blotting and (d–f) electron microscopy. Western blots with (a) anti-gB rabbit, (b) anti-MHC class I (W6/32) or (c) anti-CD63 (CLB-gran/12, 435) antibodies are shown. The same amount of each protein fraction was added to each well of the gel. Immunogold labeling of (d) gB in fraction 6 and of (e,f) MHC class I in fractions 6 and 7. The fractions were collected from the bottom of tube. Hollow arrowheads, labeled virions; filled arrowheads, exosomes. Scale bars: 200 nm (d–f).

intracellular) expression of MHC class I in HHV-6-infected cells suggests that some of them may be transported to lysosomes and degraded, as this route is the same as that used to transport particles to MVBs.

Although several host proteins are usually expressed on the surfaces of uninfected cells, they are expressed in the same intracellular compartments as those in which viral particles incorporated. Newly formed compartments

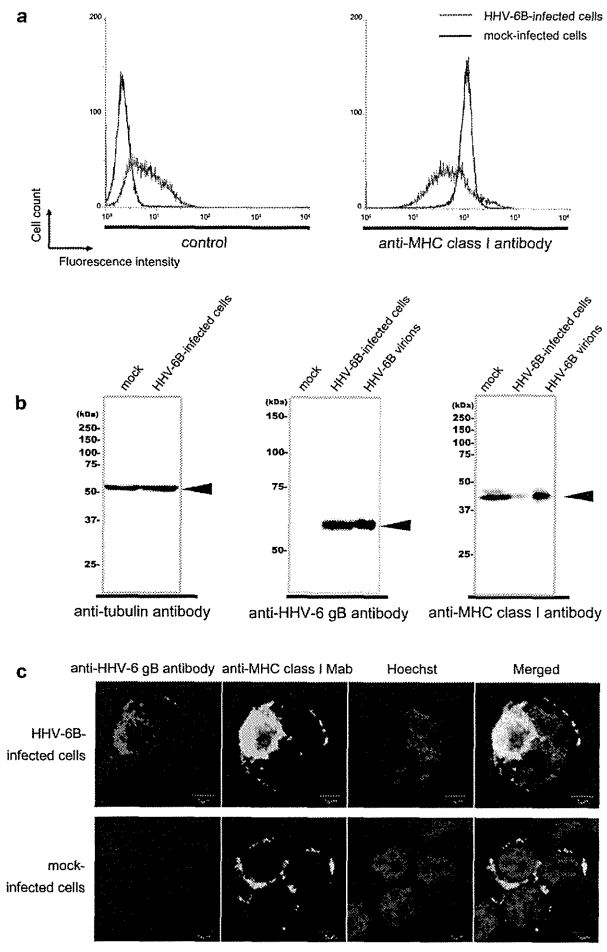

Fig. 2. Expression of MHC class I in HHV-6B-infected cells. (a) Expression of MHC class I on the surface of HHV-6B-infected cells is downregulated. HHV-6B-infected or mock-infected cells were harvested at 72 hr post-infection and fixed with 4% (w/v) paraformaldehyde. Fixed cells were stained with an anti-MHC class I antibody followed by staining with a secondary antibody prior to flow cytometric analysis. Control samples were incubated with the secondary antibody alone. Black histogram, mock-infected cells; blue histogram, HHV-6B- infected cells. (b) The total expression of MHC class I in HHV-6-infected cells was reduced. HHV-6B-infected or mock-infected cells were harvested at 72 hr post-infection and cell lysates prepared for western blotting. Purified HHV-6B virions were also used for western blotting. (c) MHC class I colocalizes with HHV-6B gB in intracellular compartments. HHV-6B-infected or mock-infected cells were harvested at 72 hr post-infection and fixed in cold acetone–methanol. Fixed cells were stained with antibodies against HHV-6 gB or MHC class I and with Hoechst33342. The stained cells were observed under a confocal microscope. The merged panels show the colocalized HHV-6 gB and MHC class I molecules. Single sections are shown. Scale bars: 5 micro meter.

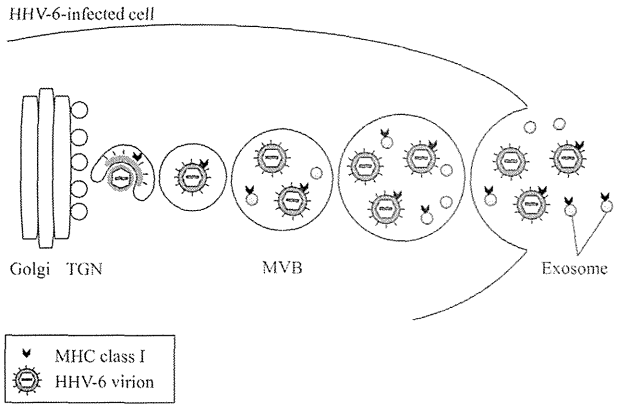

Fig. 3. Schematic representation of the fate of MHC class I molecules in HHV-6-infected cells. MHC class I molecules are transported to TGN- or post-TGN-derived vacuoles in HHV-6-infected cells and then incorporated into virions and intracellular small vesicles, which later become exosomes. Finally, MHC class I molecules are released from HHV-6-infected cells along with virions and exosomes.

within HHV-6-infected cells may show the combined characteristics of early and late endosomes. Recycling to early endosomes in HHV-6-infected cells may be modified or defective; therefore, several cellular proteins that use the same recycling system may be incorporated into virions and exosomes.

ACKNOWLEDGMENTS

We thank Dr. Kazushige Adachi (Minoh City Hospital) and Dr. Hideto Yamada (Department of Obstetrics and Gynecology, Kobe University Graduate School of Medicine) for providing the CBMCs. We also thank Ms. Eiko Moriishi (National Institute of Biomedical Innovation) for her technical support. This study was supported in part by a Grant-in-Aid for Scientific Research (B) and a Grant-in-Aid for Exploratory Research from the Japan Society for the Promotion of Science (JSPS).

DISCLOSURE

The authors declare that they have no competing interests.

REFERENCES

1. Roizmann B., Desrosiers R.C., Fleckenstein B., Lopez C., Minson A.C., Studdert M.J. (1992) The family Herpesviridae: an update. The Herpesvirus Study Group of the International Committee on Taxonomy of Viruses. *Arch Virol* **123**: 425–49.
2. Salahuddin S.Z., Ablashi D.V., Markham P.D., Josephs S.F., Sturzenegger S., Kaplan M., Halligan G., Biberfeld P., Wong-Staal F., Kramarsky B., Gallo R.C. (1986) Isolation of a new virus, HBLV, in patients with lymphoproliferative disorders. *Science* 234: 596–601.
3. Aubin J.T., Collandre H., Candotti D., Ingrand D., Rouzioux C., Burgard M., Richard S., Huraux J.M., Agut H. (1991) Several groups among human herpesvirus 6 strains can be distinguished by Southern blotting and polymerase chain reaction. *J Clin Microbiol* **29**: 367–72.
4. Campadelli-Fiume G., Guerrini S., Liu X., Foa-Tomasi L. (1993) Monoclonal antibodies to glycoprotein B differentiate human herpesvirus 6 into two clusters, variants A and B. *J Gen Virol* **74**(Pt 10) 2257–62.
5. Wyatt L.S., Balachandran N., Frenkel N. (1990) Variations in the replication and antigenic properties of human herpesvirus 6 strains. *J Infect Dis* **162**: 852–7.
6. Yamanishi K., Okuno T., Shiraki K., Takahashi M., Kondo T., Asano Y., Kurata T. (1988) Identification of human herpesvirus-6 as a causal agent for exanthem subitum. *Lancet* **1**: 1065–7.
7. Okuno T., Takahashi K., Balachandra K., Shiraki K., Yamanishi K., Takahashi M., Baba K. (1989) Seroepidemiology of human herpesvirus 6 infection in normal children and adults. *J Clin Microbiol* **27**: 651–3.
8. Ahn K., Gruhler A., Galocha B., Jones T.R., Wiertz E.J., Ploegh H.L., Peterson P.A., Yang Y., Fruh K. (1997) The ER-luminal domain of the HCMV glycoprotein US6 inhibits peptide translocation by TAP. *Immunity* **6**: 613–21.
9. Hill A., Jugovic P., York I., Russ G., Bennink J., Yewdell J., Ploegh H., Johnson D. (1995) Herpes simplex virus turns off the TAP to evade host immunity. *Nature* **375**: 411–5.

10. Tomazin R., Van Schoot N.E., Goldsmith K., Jugovic P., Sempe P., Fruh K., Johnson D.C. (1998) Herpes simplex virus type 2 ICP47 inhibits human TAP but not mouse TAP. *J Virol* **72**: 2560–3.
11. Wills M.R., Ashiru O., Reeves M.B., Okecha G., Trowsdale J., Tomasec P., Wilkinson G.W., Sinclair J., Sissons J.G. (2005) Human cytomegalovirus encodes an MHC class I-like molecule (UL142) that functions to inhibit NK cell lysis. *J Immunol* **175**: 7457–65.
12. Jones T.R., Wiertz E.J., Sun L., Fish K.N., Nelson J.A., Ploegh H.L. (1996) Human cytomegalovirus US3 impairs transport and maturation of major histocompatibility complex class I heavy chains. *Proc Natl Acad Sci USA* **93**: 11,327–33.
13. Wiertz E.J., Jones T.R., Sun L., Bogyo M., Geuze H.J., Ploegh H.L. (1996) The human cytomegalovirus US11 gene product dislocates MHC class I heavy chains from the endoplasmic reticulum to the cytosol. *Cell* **84**: 769–79.
14. Ziegler H., Thale R., Lucin P., Muranyi W., Flohr T., Hengel H., Farrell H., Rawlinson W., Koszinowski U.H. (1997) A mouse cytomegalovirus glycoprotein retains MHC class I complexes in the ERGIC/cis-Golgi compartments. *Immunity* **6**: 57–66.
15. Coscoy L., Ganem D. (2000) Kaposi's sarcoma-associated herpesvirus encodes two proteins that block cell surface display of MHC class I chains by enhancing their endocytosis. *Proc Natl Acad Sci USA* **97**: 8051–6.
16. Hudson A.W., Howley P.M., Ploegh H.L. (2001) A human herpesvirus 7 glycoprotein, U21, diverts major histocompatibility complex class I molecules to lysosomes. *J Virol* **75**: 12347–58.
17. Ishido S., Wang C., Lee B.S., Cohen G.B., Jung J.U. (2000) Downregulation of major histocompatibility complex class I molecules by Kaposi's sarcoma-associated herpesvirus K3 and K5 proteins. *J Virol* **74**: 5300–9.
18. Reusch U., Muranyi W., Lucin P., Burgert H.G., Hengel H., Koszinowski U.H. (1999) A cytomegalovirus glycoprotein re-routes MHC class I complexes to lysosomes for degradation. *EMBO J* **18**: 1081–91.
19. Hirata Y., Kondo K., Yamanishi K. (2001) Human herpesvirus 6 downregulates major histocompatibility complex class I in dendritic cells. *J Med Virol* **65**: 576–83.
20. Glosson N.L., Hudson A.W. (2007) Human herpesvirus-6A and -6B encode viral immunoevasins that downregulate class I MHC molecules. *Virology* **365**: 125–35.
21. Mori Y., Yagi H., Shimamoto T., Isegawa Y., Sunagawa T., Inagi R., Kondo K., Tano Y., Yamanishi K. (1998) Analysis of human herpesvirus 6 U3 gene, which is a positional homolog of human cytomegalovirus UL 24 gene. *Virology* **249**: 129–39.
22. Mori Y., Akkapaiboon P., Yang X., Yamanishi K. (2003) The human herpesvirus 6 U100 gene product is the third component of the gH-gL glycoprotein complex on the viral envelope. *J Virol* **77**: 2452–8.
23. Mori Y., Koike M., Moriishi E., Kawabata A., Tang H., Oyaizu H., Uchiyama Y., Yamanishi K. (2008) Human herpesvirus-6 induces MVB formation, and virus egress occurs by an exosomal release pathway. *Traffic* **9**: 1728–42.
24. Okuno T., Shao H., Asada H., Shiraki K., Takahashi M., Yamanishi K. (1992) Analysis of human herpesvirus 6 glycoproteins recognized by monoclonal antibody OHV1. *J Gen Virol* **73**(Pt 2) 443–7.
25. Tang H., Kawabata A., Takemoto M., Yamanishi K., Mori Y. (2008) Human herpesvirus-6 infection induces the reorganization of membrane microdomains in target cells, which are required for virus entry. *Virology* **378**: 265–71.
26. Kawabata A., Tang H.M., Huang H.L., Yamanishi K., Mori Y. (2009) Human herpesvirus 6 envelope components enriched in lipid rafts: evidence for virion-associated lipid rafts. *Virology J* **6**: 127.
27. Yamada M., Mugnai G., Serada S., Yagi Y., Naka T., Sekiguchi K. (2013) Substrate-attached materials are enriched with tetraspanins and are analogous to the structures associated with rear-end retraction in migrating cells. *Cell Adh Migr* **7**: 304–14.
28. Akkapaiboon P., Mori Y., Sadaoka T., Yonemoto S., Yamanishi K. (2004) Intracellular processing of human herpesvirus 6 glycoproteins Q1 and Q2 into tetrameric complexes expressed on the viral envelope. *J Virol* **78**: 7969–83.
29. Mori Y., Akkapaiboon P., Yonemoto S., Koike M., Takemoto M., Sadaoka T., Sasamoto Y., Konishi S., Uchiyama Y., Yamanishi K. (2004) Discovery of a second form of tripartite complex containing gH-gL of human herpesvirus 6 and observations on CD46. *J Virol* **78**: 4609–16.
30. Raposo G., Nijman H.W., Stoorvogel W., Liejendekker R., Harding C.V., Melief C.J., Geuze H.J. (1996) B lymphocytes secrete antigen-presenting vesicles. *J Exp Med* **183**: 1161–72.
31. Elboim M., Grodzovski I., Djian E., Wolf D.G., Mandelboim O. (2013) HSV-2 specifically down regulates HLA-C expression to render HSV-2-infected DCs susceptible to NK cell killing. *PLoS Pathog* **9**: e1003226.
32. Kubota A., Kubota S., Farrell H.E., Davis-Poynter N., Takei F. (1999) Inhibition of NK cells by murine CMV-encoded class I MHC homologue m144. *Cell Immunol* **191**: 145–51.
33. Ma G., Feineis S., Osterrieder N., Van De Walle G.R. (2012) Identification and characterization of equine herpesvirus type 1 pUL56 and its role in virus-induced downregulation of major histocompatibility complex class I. *J Virol* **86**: 3554–63.
34. Neumann L., Kraas W., Uebel S., Jung G., Tampe R. (1997) The active domain of the herpes simplex virus protein IC P47: a potent inhibitor of the transporter associated with antigen processing. *J Mol Biol* **272**: 484–92.
35. Raafat N., Sadowski-Cron C., Mengus C., Heberer M., Spagnoli G.C., Zajac P. (2012) Preventing vaccinia virus class-I epitopes presentation by HSV-ICP47 enhances the immunogenicity of a TAP-independent cancer vaccine epitope. *Int J Cancer* **131**: E659–69.
36. Said A., Azab W., Damiani A., Osterrieder N. (2012) Equine herpesvirus type 4 UL56 and UL49.5 proteins downregulate cell surface major histocompatibility complex class I expression independently of each other. *J Virol* **86**: 8059–71.
37. Vasireddi M., Hilliard J. (2012) Herpes B virus, macacine herpesvirus 1, breaks simplex virus tradition via major histocompatibility complex class I expression in cells from human and macaque hosts. *J Virol* **86**(12) 503–11.

OPEN ACCESS Freely available online

PLOS | ONE

Karyopherin Alpha2 Is Essential for rRNA Transcription and Protein Synthesis in Proliferative Keratinocytes

Noriko Umegaki-Arao[1], Katsuto Tamai[2]*, Keisuke Nimura[3], Satoshi Serada[4], Tetsuji Naka[4], Hajime Nakano[5], Ichiro Katayama[1]

1 Department of Dermatology, Osaka University Graduate School of Medicine, Osaka, Japan, **2** Department of Stem Cell Therapy Science, Osaka University Graduate School of Medicine, Osaka, Japan, **3** Division of Gene Therapy Science, Osaka University Graduate School of Medicine, Osaka, Japan, **4** National Institute of Biomedical Innovation Laboratory for Immune Signal, Osaka, Japan, **5** Department of Dermatology, Hirosaki University School of Medicine, Hirosaki, Japan

Abstract

Karyopherin proteins mediate nucleocytoplasmic trafficking and are critical for protein and RNA subcellular localization. Recent studies suggest KPNA2 expression is induced in tumor cells and is strongly associated with prognosis, although the precise roles and mechanisms of KPNA2 overexpression in proliferative disorders have not been defined. We found that KPNA2 expression is induced in various proliferative disorders of the skin such as psoriasis, Bowen's disease, actinic keratosis, squamous cell carcinoma, Paget's disease, Merkel cell carcinoma, and mycosis fungoides. siRNA-mediated KPNA suppression revealed that KPNA2 is essential for significant suppression of HaCaT proliferation under starvation conditions. Ribosomal RNA transcription and protein synthesis were suppressed by starvation combined with knockdown of KPNA (including KPNA2) expression. KPNA2 localized to the nucleolus and interacted with proteins associated with mRNA processing, ribonucleoprotein complex biogenesis, chromatin modification, and transcription, as demonstrated by tandem affinity purification and mass spectrometry. KPNA2 may be an important promoter of ribosomal RNA and protein synthesis in tumor cells.

Citation: Umegaki-Arao N, Tamai K, Nimura K, Serada S, Naka T, et al. (2013) Karyopherin Alpha2 Is Essential for rRNA Transcription and Protein Synthesis in Proliferative Keratinocytes. *PLoS ONE* 8(10): e76416. doi:10.1371/journal.pone.0076416

Editor: Andrzej T. Slominski, University of Tennessee, United States of America

Received November 9, 2012; **Accepted** August 29, 2013; **Published** October 3, 2013

Funding: This work was supported by a Grant-in-Aid of Scientific Research from the Ministry of Education, Culture, Science and Technology of Japan, and a Health and Labour Science Research Grant from the Ministry of Health, Labour and Welfare of Japan. The funders had no role in study design, data collection and analysis, decision to publish, or preparation of the manuscript.

Competing Interests: The authors have declared that no competing interests exist.

* E-mail: tamai@gts.med.osaka-u.ac.jp

Introduction

Recent studies have defined the molecular mechanisms of nucleocytoplasmic signal transduction by karyopherins (KPNs), which function as receptors for various intracellular molecules and mediate nuclear import and export during interphase. In humans, the karyopherin alpha (KPNA) family consists of at least 7 family members, all of which interact with karyopherin beta (KPNB) 1 and transport various proteins and RNAs through the nuclear pores in an energy-dependent manner [1–3]. Various extracellular environmental changes activate intracellular signaling cascades by which cells exchange activated signaling molecules between the nucleus and cytoplasm via the KPN-mediated machinery to regulate proliferation and differentiation status [2,4–6]. KPNA2 expression in human epidermal keratinocytes, but not in human dermal fibroblasts, is differentially regulated by transforming growth factor (TGF)-β_1 and interferon (IFN)-γ, both of which are established modulators of epidermal proliferation and differentiation [4]. KPNA2 also mediates the translocation of epidermal differentiation-inducing signals into the nucleus by recruiting transcription factors such as interferon regulatory factor-1 (IRF-1), thereby inducing IFN-γ-mediated epidermal differentiation [4]. Karyopherin alphas also mediate mitotic spindle assembly [7–9] and nuclear membrane formation [10]. KPNB1 is also a global regulator of mitotic spindle assembly, centrosome dynamics, nuclear membrane formation, and nuclear pore complex assembly [11,12]. Recent studies have revealed that KPNs including KPNA2 are overexpressed in various kinds of tumors such as breast cancer, cervical cancer, non-small cell lung cancer, prostate cancer, and primary cutaneous melanoma, and that expression levels in these tumors are closely associated with prognosis [13–18]. Nevertheless, the precise roles and mechanisms of KPN overexpression in proliferative disorders have not been defined.

The rate of cell growth and proliferation is proportional to the rate of protein synthesis, which is tightly linked to ribosome biologics [19,20]. RNA synthesis and ribosome construction occur in the nucleolus and their control is important for regulating protein synthesis; however, the precise mechanisms and roles of karyopherins in regulating rRNA and protein synthesis remain unclear.

We report KPNA2 induction in proliferation disorders regardless of malignancy, and suggest KPNA2 regulates rRNA transcription and general protein synthesis in the nucleolus to maintain proliferation.

Materials and Methods

Skin Samples

Written informed consent was obtained from all patients, and the study protocol was approved by Medical Ethics Committee of Osaka University.

Cell Culture

HaCaT cells, an immortalized, nontumorigenic keratinocyte cell line, were cultured in Dulbecco's modified Eagle's medium (DMEM; Nacalai Tesque) containing 10% fetal bovine serum (FBS) at 37°C under 5% CO_2-95% air.

RNA Purification and Reverse Transcription-quantitative Polymerase Chain Reaction

Total RNA was isolated from HaCaT cells with an RNA isolation kit (Qiagen) and reverse transcribed with SuperScript III reverse transcriptase (Invitrogen). Expression of prc-rRNA was determined by using Power SYBR green PCR Master Mix (Applied Biosystems) according to the manufacturer's protocol. β-Actin was used to normalize target gene expression. PCR amplification was performed with 5′-ATCGTCCACCGCA-AATGCTTCTA-3′ and 5′-AGCCATGCCAATCTCATCTT-GTT-3′ for β-actin and 5′-GAACGGTGGTGTGTCGTTC-3′ and 5′-GCGTCTCGTCTCGTCTCACT-3′ for pre-rRNA [21]. PCR cycling conditions were 40 cycles of denaturing at 92°C for 15 sec and annealing at 60°C for 60 sec on an ABI Prism 7000 sequence detection system (Applied Biosystems).

Small Interfering RNA and Plasmid DNA Transfection

Small interfering RNAs (siRNAs) specific for KPNA1, 2, 3, and 4 and the control stealth siRNA were obtained from Invitrogen. Cells (1.5×10^6) were transfected with 100 ng siRNAs mixture using the Neon transfection system (Invitrogen). We performed the knockdown studies with each siRNA, which ensured more than 50–70% suppression of KPNA2 mRNA and protein.

MTS

[3-(4,5-dimethylthiazol-2-yl)-5(3-carboxymethoxyphenyl)-2-(4-sulfophenyl)-2H-tetrazolium] assay. HaCaT cells induced with each siRNA were seeded at their optimal cell density (7×10^4 cells/well) in 96-well microtiter plates and incubated to allow cell attachment. After 6 h, cells were incubated with 0.1% FBS DMEM for 24, 48, 72, and 120 h. At the end of each incubation period, cell viability was determined by using the CellTiter 96® AQ_{ueous} Non-Radioactive Cell Proliferation Assay (Promega) according to the manufacturer's instructions. Samples were incubated at 37°C in a humidified 5% CO_2 atmosphere for 1 h. Absorbance was measured at 490 nm using a microplate reader.

Immunohistochemistry

Slides of skin biopsies in paraffin blocks were stained with hematoxylin and eosin (HE) and anti-human KPNA2 mouse monoclonal antibody (BD Biosciences) (1:1000).

Immunofluorescence

HaCaT cells were fixed in 4% formaldehyde in phosphate-buffered saline (PBS) for 40 min. After rinsing twice with PBS, the cells were permeabilized in 0.5% Triton X-100 in PBS for 60 s and blocked with 2% skim milk overnight at 4°C. The cells were incubated with anti-UBF (Santa Cruz) and anti-KPNA2 antibodies for 1 h and stained with Alexa Fluor 546 goat anti-rabbit IgG and Alexa Fluor 488 goat anti-mouse IgG secondary antibodies (1:1000; Invitrogen A-11035 and A-11029) for 1 h. After washing with PBS, cells were counterstained with 0.5 mg/mL 4′, 6′-diamidino-2-phenylindole (DAPI) and mounted with Vectashield mounting medium (Vector Laboratories). Cells were analyzed using a Radiance 2100 confocal scanning-laser microscope (Bio-Rad) equipped with an Eclipse TE-2000 inverted microscope

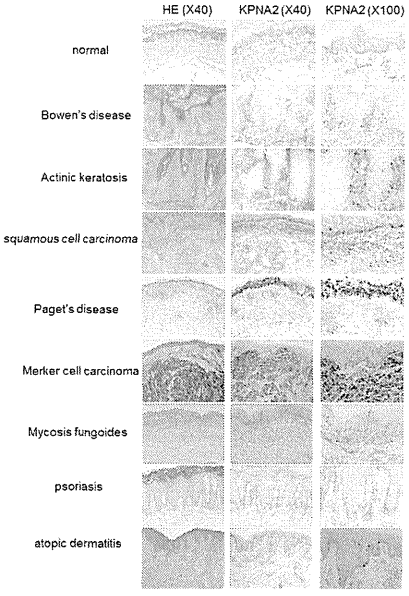

Figure 1. Overexpression of KPNA2 in proliferating cells. Immunohistochemistry showed KPNA2 was uniformly expressed throughout the epidermis in healthy skin, although KPNA2 overexpression was observed in the basal layer in psoriasis. In contrast, very few cells exhibited KPNA2 staining in the basal cells of atopic dermatitis. KPNA2 overexpression was observed in the tumor cells of Bowen's disease, actinic keratosis, squamous cell carcinoma, Paget's disease, Merkel cell carcinoma, and mycosis fungoides.
doi:10.1371/journal.pone.0076416.g001

(Nikon) or a Nikon A1 confocal scanning-laser microscope equipped with a Nikon Eclipse Ti inverted microscope.

Tandem Affinity Purification (TAP) and Mass Spectrometry

KPNA2 and GFP cDNAs were introduced into pCAGIP-gw-TAP by using Gateway technology (Invitrogen). KPNA2-TAP and GFP-TAP complexes were purified from HaCaT cell extracts using TAP technology [22,23]. Proteins were separated by SDS-PAGE and stained with the Silver Stain MS Kit (Wako Pure Chemical Industries). Protein bands were excised from the gel and digested with trypsin (Promega) [24]. NanoLC-MS/MS analyses were performed on a LTQ-Orbitrap XL mass spectrometer (Thermo Fisher Scientific) equipped with a nano-ESI source (AMR) and coupled to a Paradigm MG4 pump (Michrom Bioresources) and an autosampler (HTC PAL, CTC Analytics). A spray voltage of 1800 V was applied. The peptide mixture was separated on a MagicC18AQ column (100 μm×150 mm, 3.0 μm particle size, 300 Å, Michrom Bioresources) with a flow rate of 500 nl/min. A linear gradient of 5% to 45% B in 30 min, 45% to 95% B in 0.1 min, and 95% B for 2 min and 5% B was employed

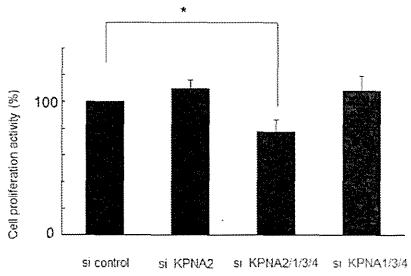

Figure 2. Suppression of cell growth by combined KPNA knockdown. Under starvation conditions (0.1% FBS), siRNA-mediated knockdown of KPNA2, 1, 3, and 4 suppressed cell growth after 120 h (*$p<0.05$). Only KPNA2 siRNA subtraction produced no change in proliferation.
doi:10.1371/journal.pone.0076416.g002

(A = 0.1% formic acid in 2% acetonitrile, B = 0.1% formic acid in 90% acetonitrile). Intact peptides were detected in the Orbitrap at 60,000 resolutions. For LC-MS/MS analysis, 6 precursor ions were selected for MS/MS scans in a data-dependent acquisition mode following each full scan (m/z, 350–1500). A lock mass function was used for the LTQ-Orbitrap to obtain constant mass accuracy during gradient analysis.

Peptides and proteins were identified by automated database searching the Swiss-Prot protein database (version 57.14x) with the MASCOT search program (version 1.0; Matrix Science) and a precursor mass tolerance of 10 p.p.m., a fragment ion mass tolerance of 0.8 Da, and strict trypsin specificity, allowing for up to 2 missed cleavages. Carbamidomethylation of cysteine was set as a fixed modification and oxidation of methionines was allowed as a variable modification.

Metabolic Labeling

HaCaT cells were labeled for 2 h with 100 mCi ^{35}S-methionine in methionine-free DMEM (Gibco) supplemented with 10% dialyzed serum. Protein was extracted with TNE buffer containing 50 mM Tris-HCl at pH 7.4, 150 mM NaCl, 2 mM EDTA, and 0.5% NP-40, then resuspended in 1% sodium dodecyl sulfate and boiled for 10 min at 100°C. Radioactivity was measured with a Beckmann Coulter liquid scintillation counter and normalized to protein content.

Transient Transfection and Luciferase Assay

The human pre-rRNA-luc vector was kindly provided by Dr. Samson Jacob [25]. HaCaT cells induced with each siRNA were seeded in a 12-well plate and transfected with 0.34 μg human-pre-rRNA-luc plasmid and Fugene 6 transfection reagent (Roche). The luciferase reporter assay was performed using a commercial luciferase assay kit (Promega). Data were normalized to the protein concentration.

Statistical Analysis

All data and results were confirmed in at least 3 independent experiments. Statistical significance was determined by one-way analysis of variance (ANOVA).

Results

KPNA2 Overexpression in Proliferative Disorders of the Skin

To investigate KPNA2 expression in various epidermal-proliferative disorders of the skin, immunohistochemical staining of KPNA2 was performed on biopsy specimens of epidermal tumors as well as psoriasis and atopic dermatitis, which are inflammatory skin diseases with higher and lower epidermal proliferation, respectively. KPNA2 staining was faint and homogeneous without significant nuclear accumulation in healthy epidermis. In contrast, there was marked KPNA2 staining in the nuclei and cytoplasm of malignant cells in several skin tumors with different prognoses including Bowen's disease, actinic keratosis, squamous cell carcinoma (SCC), Paget's disease, Merkel cell carcinoma, and Mycosis fungoides. In malignant cells of SCC *in situ* such as Bowen's disease and actinic keratosis as with well prognosis, KPNA2 expressed predominantly in the basal layer. In contrast, established SCC showed rather intense and diffuse expression of KPNA2 in the malignant cells. Non-squamous cell malignant tumors of the skin including Paget's disease, Merkel cell carcinoma, and mycosis fungoides also showed diffuse, intense staining of KPNA2, indicating significantly higher expression in skin malignancy. Marked staining of KPNA2 was also observed in psoriatic skin, but was limited to the cytoplasm of basal layer keratinocytes. In contrast, very few but significant numbers of KPNA2-positive keratinocytes were observed in the basal lesions of atopic dermatitis, particularly in the inflamed proliferating lesions (**Figure 1**).

Contribution of KPNA2 and other KPNAs to Keratinocyte Cell Growth

To assess the role of KPNs in keratinocyte proliferation, HaCaT cell growth in culture was assessed by MTS assay after siRNA-mediated knockdown of KPNs. In culture medium containing 10% FBS, growth was significantly suppressed by KPNB1 knockdown [13]; however, knockdown of other KPNAs produced no significant effect (data not shown). In starved culture medium with 0.1% FBS, HaCaT cell growth was significantly suppressed by siRNA knockdown of KPNA1, 2, 3, and 4, suggesting adequate expression of KPNAs may be required for growth maintenance, especially in starved cells such as cancer cells. About 20% of HaCaT keratinocyte growth was suppressed 120 h after KPNA knockdown. KPNA siRNAs were individually subtracted from the siRNA cocktail to investigate the contribution of each KPNA to growth suppression. Interestingly, only KPNA2 siRNA subtraction resulted in the significant recovery of cell growth up to the control level (**Figure 2**), while removal of the other KPNA siRNAs did not affect growth suppression (data not shown). KPNA2 knockdown alone had no significant growth suppression effect, suggesting the other KPNAs are redundant. These data suggest KPNAs complement each other during cell growth, but KPNA2 may be essential for maintaining cell proliferation under starvation conditions.

Association of KPNA2 with Ribosomal Proteins in the Nucleolus

To identify proteins that interact with KPNA2 in HaCaT keratinocytes, we used the TAP method, which enabled us to easily isolate and purify proteins bound to the stably expressed TAP-tagged target recombinant protein [22,23]. Proteins associated with the KPNA2-TAP complex were isolated from the nuclei and cytoplasm of KPNA2-TAP-expressing HaCaT cells, separated

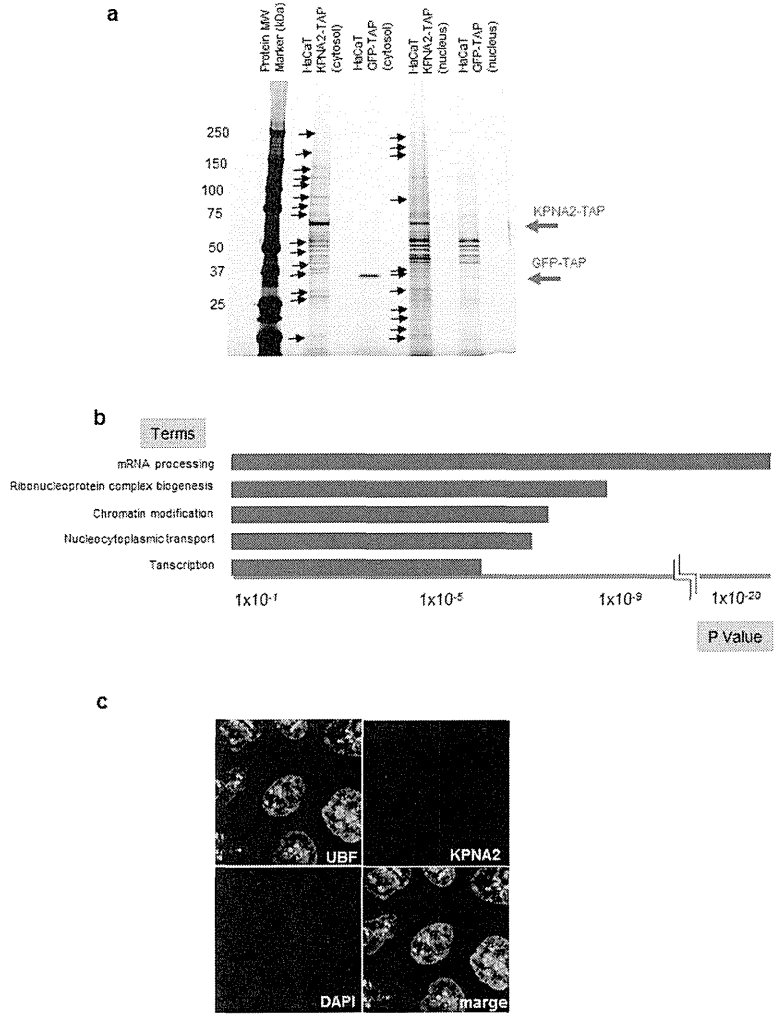

Figure 3. Detection and analysis of proteins that interact with KPNA2 and localization of KPNA2 in the nucleolus. Proteins that interact with KPNA2 in the cytoplasm and nucleus were purified using the TAP method and detected by silver staining. Proteins marked with arrows were analyzed by LC/MS/MS. HaCaT cells expressing GFP-TAP were used to detect nonspecific interactions. **a)** The results of LC/MS/MS were analyzed by pathway analysis using reactome (http://www.reactome.org). The categories of "mRNA processing", "ribonucleoprotein complex biogenesis", "chromatin modification," and "transcription" were the most significantly represented pathways. **b)** Immunohistochemistry revealed KPNA2 co-localization with UBF, a nucleolar marker.
doi:10.1371/journal.pone.0076416.g003

Table 1. Lists of proteins analyzed by pathway analysis.

mRNA processing	
RALY	RNA-binding protein Raly
NCBP1	Nuclear cap-binding protein subunit 1
RNMT	mRNA cap guanine-N7 methyltransferase
GAR1	H/ACA ribonucleoprotein complex subunit 1
PABPC4	PABPC4 protein
MLH1	DNA mismatch repair protein Mlh1
YBX1	Nuclease-sensitive element-binding protein 1
SRRT	Serrate RNA effector molecule homolog
DDX17	Probable ATP-dependent RNA helicase DDX17
RRP1B	Ribosomal RNA processing protein 1 homolog B
PCBP1	Poly(rC)-binding protein 1
PCBP2	Poly(rC)-binding protein 2
SFRS9	Splicing factor, arginine/serine-rich 9
PABPC1	Polyadenylate-binding protein 1
NSUN2	tRNA (cytosine-5-)-methyltransferase NSUN2
KRR1	KRR1 small subunit processome component homolog
DHX9	ATP-dependent RNA helicase A
RRP1	Ribosomal RNA processing protein 1 homolog B
DDX1	ATP-dependent RNA helicase DDX1
HNRNPU	Heterogeneous nuclear ribonucleoprotein U
TTF2	Transcription termination factor 2
SFRS3	Splicing factor, arginine/serine-rich 3
PHAX	Phosphorylated adapter RNA export protein
NOP2	Putative ribosomal RNA methyltransferase NOP2
RPS16	RPS16 protein
SNRNP200	U5 small nuclear ribonucleoprotein 200 kDa helicase
SYF2	Pre-mRNA-splicing factor SYF2
NOP56	NOP56 protein
RBM14	RNA-binding protein 14
BAT1	Spliceosome RNA helicase BAT1
ADAR	Double-stranded RNA-specific adenosine deaminase
KIAA1429	Protein virilizer homolog
Ribonucleoprotein complex biogenesis	
NCBP1	Nuclear cap-binding protein subunit 1
KRR1	KRR1 small subunit processome component homolog
RRP1	Ribosomal RNA processing protein 1 homolog B
GAR1	H/ACA ribonucleoprotein complex subunit 1
NIP7	60 S ribosome subunit biogenesis protein NIP7 homolog
DDX1	ATP-dependent RNA helicase DDX1
PHAX	Phosphorylated adapter RNA export protein
NOP2	Putative ribosomal RNA methyltransferase NOP2
RPS16	RPS16 protein
RRP1B	Ribosomal RNA processing protein 1 homolog B
SNRNP200	U5 small nuclear ribonucleoprotein 200 kDa helicase
SFRS9	Splicing factor, arginine/serine-rich 9
NOP56	NOP56 protein
Chromatin modification	

Table 1. Cont.

mRNA processing	
ING5	Inhibitor of growth protein 5
RBBP4	Histone-binding protein RBBP4
RBBP7	Histone-binding protein RBBP7
ARID2	AT-rich interactive domain-containing protein 2
CHD8	Chromodomain-helicase-DNA-binding protein 8
HDAC2	Histone deacetylase 2
HDAC1	Histone deacetylase 1
ASH1L	Probable histone-lysine N-methyltransferase ASH1L
BRDT	Bromodomain testis-specific protein
RBM14	RNA-binding protein 14
BCOR	BCL-6 corepressor
CHD4	Chromodomain-helicase-DNA-binding protein 4
MLL2	Histone-lysine N-methyltransferase MLL2
Nucleocytoplasmic transport	
PHAX	Phosphorylated adapter RNA export protein
NCBP1	Nuclear cap-binding protein subunit 1
UPF1	Regulator of nonsense transcripts 1
SET	Protein SET
GLE1	Nucleoporin GLE1
NUPL2	Nucleoporin-like protein 2
TPR	Nucleoprotein
KPNA2	Importin subunit alpha-2
KPNB1	Importin subunit beta-1
BAT1	Spliceosome RNA helicase BAT1
Transcription	
ING5	Inhibitor of growth protein 5
NMI	N-myc-interactor
FOXK1	Forkhead box protein K1
FOXM1	Forkhead box protein M1
CCNT1	Cyclin-T1
ARID2	AT-rich interactive domain-containing protein 2
YBX1	Nuclease-sensitive element-binding protein 1
CNOT4	CCR4-NOT transcription complex subunit 4
YBX2	Y-box-binding protein 2
CHD8	Chromodomain-helicase-DNA-binding protein 8
ASH2L	Set1/Ash2 histone methyltransferase complex subunit ASH2
BCOR	BCL-6 corepressor
EWSR1	RNA-binding protein EWS
CHD4	Chromodomain-helicase-DNA-binding protein 4
MLL2	Histone-lysine N-methyltransferase MLL2
ASXL3	Putative Polycomb group protein ASXL3
TAF4	Transcription initiation factor TFIID subunit 4
RBBP4	Histone-binding protein RBBP4
TAF6	Transcription initiation factor TFIID subunit 6
POLR1A	DNA-directed RNA polymerase I subunit RPA1
MED12	Mediator of RNA polymerase II transcription subunit 12
CSDA	DNA-binding protein A

doi:10.1371/journal.pone.0076416.t001

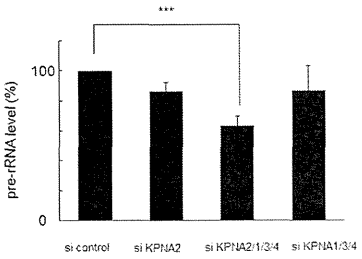

Figure 4. Suppression of ribosomal RNA synthesis by combined KPNA knockdown. Under starvation conditions (0.1% fetal bovine serum), siRNA-mediated knockdown of KPNA2, 1, 3, and 4 significantly suppressed ribosomal RNA synthesis analyzed by reverse transcription-quantitative polymerase chain reaction (***$p<0.01$). The amount of pre-ribosomal RNA was reduced by about 37% after 72 h.
doi:10.1371/journal.pone.0076416.g004

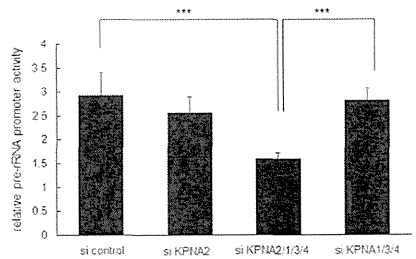

Figure 6. Suppression of the pre-ribosomal RNA promoter by combined KPNA knockdown. Under starvation conditions (0.1% fetal bovine serum), siRNA-mediated knockdown of KPNA2, 1, 3, and 4 significantly suppressed pre-rRNA promoter activity after 24 h (***$p<0.01$).
doi:10.1371/journal.pone.0076416.g006

by SDS-PAGE, and silver stained. HaCaT cells expressing GFP-TAP were used as a negative control (**Figure 3a**). KPNA2-TAP-associated proteins extracted from the silver-stained gel were identified by mass spectrometry. Numerous proteins were analyzed by reactome (http://www.reactome.org) to investigate their biological relationships. Pathway analysis revealed that the proteins interacting with KPNA2 were associated with mRNA processing, ribonucleoprotein complex biogenesis, chromatin modification, and transcription, all of which are essential for cell activities including cell growth (**Figure 3b, Table 1**). Interestingly, significant numbers of ribosomal proteins were listed as associated with KPNA2. Furthermore, immunofluorescence staining of KPNA2 in cultured HaCaT keratinocytes demonstrated co-localization of KPNA2 with UBF in the nucleoli, suggesting a role of KPNA2 for maintaining rRNA function (**Figure 3c**).

Contribution of KPNA2 to Protein Synthesis and Ribosomal RNA Transcription

Because the nucleolus is specifically responsible for rRNA transcription and maintenance of gene expression/transcription and mRNA processing, we hypothesized that KPNA2 in the nucleoli may regulate rRNA transcription to maintain cell growth under starvation conditions. To test this hypothesis, the siRNA cocktail was again applied to knockdown KPNAs to observe the effect on pre-rRNA transcription in starved HaCaT keratinocytes. Knockdown of all KPNAs reduced pre-rRNA levels as measured by RT-qPCR. In the 72 h after treatment with the siRNA cocktail, pre-rRNA expression was reduced by about 40%. Subtraction of KPNA2 siRNA restored pre-rRNA expression. The other KPNAs did not contribute to pre-rRNA expression. Treatment with KPNA2 siRNA alone had no significant effect, suggesting a redundant mechanism with other KPNAs (**Figure 4**). Protein synthesis in HaCaT keratinocytes was also reduced, corresponding to the suppression of pre-rRNA expression (**Figure 5**). The pre-rRNA promoter was also suppressed by KPNA knockdown after 24 h (**Figure 6**). Fluorescence-activated cell sorting of HaCaT cells before and after KPNA knockdown showed no significant change in the cell cycle pattern (data not shown). These data suggest KPNA2 might positively regulate rRNA transcription in the nucleolus, maintaining cell growth by ensuring transcription and translation directly or indirectly.

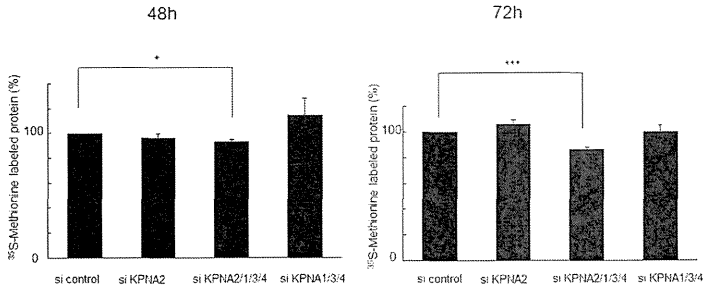

Figure 5. Suppression of protein synthesis by combined KPNA knockdown. Under starvation conditions (0.1% fetal bovine serum), siRNA-mediated knockdown of KPNA2, 1, 3, and 4 significantly suppressed protein synthesis after 48 h (*$p<0.05$) and 72 h (***$p<0.01$), as demonstrated by metabolic labeling with ^{35}S-methionine.
doi:10.1371/journal.pone.0076416.g005

Discussion

In this study, KPNA2 was overexpressed in proliferating disorders of the skin and interacted with many kinds of proteins that control transcription and gene expression directly and indirectly. This was the first report to show that KPNA2 is essential for cell growth in terms of rRNA and protein synthesis under starvation conditions.

KPNA2 overexpression in several skin malignancies is associated with varying prognoses. In the basal cells of psoriasis, KPNA2 expression was diffusely up-regulated in comparison to atopic dermatitis. Thus, KPNA2 expression might be induced in cells in which proliferation has been activated. Comparing Bowen's disease and actinic keratosis, which are known as SCC *in situ*, KPNA2 was remarkably and diffusely overexpressed. KPNA2 may therefore be a tumor marker with utility as a prognostic factor of proliferative activity in skin malignancies, although we have insufficient sample sizes to determine significance. Previous reports have demonstrated KPNA2 overexpression in various tumors cells *in vitro* and *in vivo*; elevated KPNA2 and KPNB1 expression in cancer cells correlates with altered transcriptional regulation associated with deregulated E2F/Rb activities [26]. Some studies have indicated that higher KPNA2 expression in tumor cell nuclei shortens patient survival, although the mechanisms and precise roles of KPNA2 in the tumor cells remained unclear [16,17]. Researchers also hypothesized that KPNA2-mediated nuclear transport of proteins necessary for maintaining cell proliferation, such as transcription factors, promote tumor cell growth. In this context, KPNA2 was shown to interact with NBS1 (Nijmegen breakage syndrome 1), a key regulator of the MRE11/RAD50/NBS1 complex. NBS1 promotes tumorigenesis by binding and activating the phosphatidylinositol 3-kinase/AKT pathway [27]. Interestingly, siRNA-medicated KPNA2 knockdown studies revealed a different cellular response to KPNA2 inhibition in prostate and cervical cancer cell lines. In prostate cell line PC3, proliferation and viability were significantly reduced when KPNA2 expression was inhibited, whereas there was no significant change in a cervical cancer cell line. This difference could be due to tissue-specific tumor etiologies [13,17].

In this study, we characterized KPNA2-binding proteins *in situ* in immortalized HaCaT keratinocytes. In silico gene ontology indicated a significant relationship between KPNA2 binding proteins and mRNA processing, ribonucleoprotein complex biogenesis, chromatin modification, and transcription. KPNA2 interacted with various ribosomal proteins and heterogeneous nuclear ribonucleoproteins directly or indirectly and was located in the nucleolus, the site of pre-rRNA transcription and processing and ribosome assembly. rRNA synthesis, the first event in ribosome synthesis, is a fundamental determinant of a cell's capacity to grow and proliferate. Ribosomal RNA genes (rDNAs) are transcribed with high efficiency and the complex regulation of rRNA synthesis is responsive to general metabolism and specific environmental challenges [20,28]. Serum starvation is also a well-established approach to inducing a broad range of cellular stress. TAP analysis revealed that KPNA2 associates with numerous ribosomal RNA synthesis-related proteins including RNA polymerase I subunit, rRNA methyl transferase, rRNA subunit biogenesis protein, and rRNA processing proteins. Furthermore, KPNA2 accumulates in the nucleolus and contributes to rRNA transcription *in vitro*. These lines of evidence suggest KPNA2 may serve important roles as a canonical nuclear transporter and to ensure rRNA biogenesis in proliferating cells. In this context, enhanced KPNA2 expression in malignant and inflammatory keratinocytes may positively regulate their proliferating capacity by supporting rRNA synthesis, which is indispensable. In malignant cells, the poor prognosis indicated by nuclear KPNA2 accumulation may be associated with KPNA2 retention in response to cellular stress and increasing rRNA synthesis or changing gene expression.

KPNA subtypes exhibit different abilities to interact with specific NLS-containing cargos and in various expression patterns in cells and tissues. KPNA2 is highly expressed in undifferentiated embryonic stem cells and down-regulated during neural differentiation, indicating that proper expression of KPNA2 is required for embryonic stem cells to maintain their undifferentiated state [29]. KPNs are also complementary because they are indispensable for cellular proliferation and differentiation. We previously examined the effect of KPNA2 siRNA subtraction on RNA expression in normal human keratinocytes by microarray analysis [4]; however, there was no increases of more than 2 fold in any other KPNs including KPNA1, 3, 4, and KPNB1 (data not shown).

In this study, KPNA2 was essential for cell growth related to rRNA and protein synthesis under starvation conditions; however, there was no significant change when only KPNA2 was knocked down. Combined knockdown of KPNA2, 1, 3, and 4 was needed to suppress cell growth and KPNA2 was indispensable. Even under these conditions, growth suppression was gradual and mild over 120 h. Furthermore, combined knockdown of KPNAs mildly suppressed the synthesis of rRNA and proteins after 72 h. These results indicated that KPNAs might play complementary roles with sufficient reserves.

Further studies are needed to clarify the additional function of KPNA2 in cell proliferation, which would be a focus for a new treatment to regulate KPNA2.

Acknowledgments

We sincerely appreciate the kind support of Prof. Yasufumi Kaneda. We also thank Ms. Eriko Nobuyoshi and Ms. Sayaka Matsumura for technical support with immunohistochemistry and reverse transcription-quantitative polymerase chain reaction.

Author Contributions

Conceived and designed the experiments: NU KT KN TN. Performed the experiments: NU SS. Analyzed the data: NU KT KN TN IK. Contributed reagents/materials/analysis tools: HN IK. Wrote the paper: NU KT.

References

1. Pemberton LF, Paschal BM (2005) Mechanisms of receptor-mediated nuclear import and nuclear export. Traffic 6: 187–198.
2. Yasuhara N, Oka M, Yoneda Y (2009) The role of the nuclear transport system in cell differentiation. Semin Cell Dev Biol 20: 590–599.
3. Yasuda Y, Miyamoto Y, Yamashiro T, Asally M, Masui A, et al. (2012) Nuclear retention of importin alpha coordinates cell fate through changes in gene expression. EMBO J 31: 83–94.
4. Umegaki N, Tamai K, Nakano H, Moritsugu R, Yamazaki T, et al. (2007) Differential regulation of karyopherin alpha 2 expression by TGF-beta1 and IFN-gamma in normal human epidermal keratinocytes: evident contribution of KPNA2 for nuclear translocation of IRF-1. J Invest Dermatol 127: 1456–1464.
5. Freire J, Covelo G, Sarandeses C, Diaz-Jullien C, Freire M (2001) Identification of nuclear-import and cell-cycle regulatory proteins that bind to prothymosin alpha. Biochem Cell Biol 79: 123–131.
6. Hall MN, Griffin CA, Simionescu A, Corbett AH, Pavlath GK (2011) Distinct roles for classical nuclear import receptors in the growth of multinucleated muscle cells. Dev Biol 357: 248–258.
7. Schatz CA, Santarella R, Hoenger A, Karsenti E, Mattaj IW, et al. (2003) Importin alpha-regulated nucleation of microtubules by TPX2. EMBO J 22: 2060–2070.
8. Gruss OJ, Carazo-Salas RE, Schatz CA, Guarguaglini G, Kast J, et al. (2001) Ran induces spindle assembly by reversing the inhibitory effect of importin alpha on TPX2 activity. Cell 104: 83–93.
9. Ems-McClung SC, Zheng Y, Walczak CE (2004) Importin alpha/beta and Ran-GTP regulate XCTK2 microtubule binding through a bipartite nuclear localization signal. Mol Biol Cell 15: 46–57.
10. Askjaer P, Galy V, Hannak E, Mattaj IW (2002) Ran GTPase cycle and importins alpha and beta are essential for spindle formation and nuclear envelope assembly in living Caenorhabditis elegans embryos. Mol Biol Cell 13: 4355–4370.
11. Harel A, Forbes DJ (2004) Importin beta: conducting a much larger cellular symphony. Mol Cell 16: 319–330.
12. Rotem A, Gruber R, Shorer H, Shaulov L, Klein E, et al. (2009) Importin beta regulates the seeding of chromatin with initiation sites for nuclear pore assembly. Mol Biol Cell 20: 4031–4042.
13. van der Watt PJ, Maske CP, Hendricks DT, Parker MI, Denny L, et al. (2009) The Karyopherin proteins, Crm1 and Karyopherin beta1, are overexpressed in cervical cancer and are critical for cancer cell survival and proliferation. Int J Cancer 124: 1829–1840.
14. Winnepenninckx V, Lazar V, Michiels S, Dessen P, Stas M, et al. (2006) Gene expression profiling of primary cutaneous melanoma and clinical outcome. J Natl Cancer Inst 98: 472–482.
15. Wang CI, Wang CL, Wang CW, Chen CD, Wu CC, et al. (2011) Importin subunit alpha-2 is identified as a potential biomarker for non-small cell lung cancer by integration of the cancer cell secretome and tissue transcriptome. Int J Cancer 128: 2364–2372.
16. Gluz O, Wild P, Meiler R, Diallo-Danebrock R, Ting E, et al. (2008) Nuclear karyopherin alpha2 expression predicts poor survival in patients with advanced breast cancer irrespective of treatment intensity. Int J Cancer 123: 1433–1438.
17. Mortezavi A, Hermanns T, Seifert HH, Baumgartner MK, Provenzano M, et al. (2011) KPNA2 expression is an independent adverse predictor of biochemical recurrence after radical prostatectomy. Clin Cancer Res 17: 1111–1121.
18. Noetzel E, Rose M, Bornemann J, Gajewski M, Knuchel R, et al. (2012) Nuclear transport receptor karyopherin-alpha2 promotes malignant breast cancer phenotypes in vitro. Oncogene 31: 2101–2114.
19. Tanaka Y, Okamoto K, Teye K, Umata T, Yamagiwa N, et al. (2010) JmjC enzyme KDM2A is a regulator of rRNA transcription in response to starvation. EMBO J 29: 1510–1522.
20. Grummt I (2003) Life on a planet of its own: regulation of RNA polymerase I transcription in the nucleolus. Genes Dev 17: 1691–1702.
21. Murayama A, Ohmori K, Fujimura A, Minami H, Yasuzawa-Tanaka K, et al. (2008) Epigenetic control of rDNA loci in response to intracellular energy status. Cell 133: 627–639.
22. Rigaut G, Shevchenko A, Rutz B, Wilm M, Mann M, et al. (1999) A generic protein purification method for protein complex characterization and proteome exploration. Nat Biotechnol 17: 1030–1032.
23. Nimura K, Ura K, Shiratori H, Ikawa M, Okabe M, et al. (2009) A histone H3 lysine 36 trimethyltransferase links Nsd2-5 to Wolf-Hirschhorn syndrome. Nature 460: 287–291.
24. Shevchenko A, Wilm M, Vorm O, Mann M (1996) Mass spectrometric sequencing of proteins silver-stained polyacrylamide gels. Anal Chem 68: 850–858.
25. Ghoshal K, Majumder S, Datta J, Motiwala T, Bai S, et al. (2004) Role of human ribosomal RNA (rRNA) promoter methylation and of methyl-CpG-binding protein MBD2 in the suppression of rRNA gene expression. J Biol Chem 279: 6783–6793.
26. van der Watt PJ, Ngarande E, Leaner VD (2011) Overexpression of Kpnbeta1 and Kpnalpha2 importin proteins in cancer derives from deregulated E2F activity. PLoS One 6: e27723.
27. Teng SC, Wu KJ, Tseng SF, Wong CW, Kao L (2006) Importin KPNA2, NBS1, DNA repair and tumorigenesis. J Mol Histol 37: 293–299.
28. Moss T (2004) At the crossroads of growth control: making ribosomal RNA. Curr Opin Genet Dev 14: 210–217.
29. Yasuhara N, Shikazaki N, Tanaka S, Nagai M, Kamikawa Y, et al. (2007) Triggering neural differentiation of ES cells by subtype switching of importin-alpha. Nat Cell Biol 9: 72–79.

Cancer Science
The official journal of the Japanese Cancer Association JCA

Molecular mechanism underlying the antiproliferative effect of suppressor of cytokine signaling-1 in non-small-cell lung cancer cells

Kazuki Shimada,[1,2] Satoshi Serada,[1] Minoru Fujimoto,[1] Shintaro Nomura,[3] Rie Nakatsuka,[4] Emi Harada,[1] Kota Iwahori,[1,2] Isao Tachibana,[2] Tsuyoshi Takahashi,[4] Atsushi Kumanogoh,[2] Tadamitsu Kishimoto[5] and Tetsuji Naka[1,6]

[1]Laboratory for Immune Signal, National Institute of Biomedical Innovation, Osaka; [2]Department of Respiratory Medicine, Allergy and Rheumatic Diseases, Osaka University Graduate School of Medicine, Osaka; [3]Faculty of Animal Bioscience, Nagahama Institute of Bio-Science and Technology, Shiga; [4]Department of Surgery, Osaka University Graduate School of Medicine, Osaka; [5]Laboratory of Immune Regulation, Osaka University Graduate School of Frontier Biosciences, Osaka, Japan

(Received March 21, 2013/Revised July 28, 2013/Accepted August 12, 2013/Accepted manuscript online August 21, 2013/Article first published online September 19, 2013)

Lung cancer (LC) is the major cause of death by cancer and the number of LC patients is increasing worldwide. This study investigated the therapeutic potential of gene delivery using suppressor of cytokine signaling 1 (SOCS-1), an endogenous inhibitor of intracellular signaling pathways, for the treatment of LC. To examine the antitumor effect of SOCS-1 overexpression on non-small-cell lung cancer (NSCLC) cells, NSCLC cells (A549, LU65, and PC9) were infected with adenovirus-expressing SOCS-1 vector. The cell proliferation assay showed that A549 and LU65, but not PC9, were sensitive to *SOCS-1* gene-mediated suppression of cell growth. Although JAK inhibitor I could also inhibit proliferation of A549 and LU65 cells, *SOCS-1* gene delivery appeared to be more potent as SOCS-1 could suppress focal adhesion kinase and epidermal growth factor receptor, as well as the JAK/STAT3 signaling pathway. Enhanced phosphorylation of the p53 protein was detected by means of phospho-kinase array in SOCS-1 overexpressed A549 cells compared with control cells, whereas no phosphorylation of p53 was observed when JAK inhibitor I was used. Furthermore, treatment with adenoviral vector AdSOCS-1 *in vivo* significantly suppressed NSCLC proliferation in a xenograft model. These results suggest that the overexpression of *SOCS-1* gene is effective for antitumor therapy by suppressing the JAK/STAT, focal adhesion kinase, and epidermal growth factor receptor signaling pathways and enhancing p53-mediated antitumor activity in NSCLC. (*Cancer Sci* 2013; 104: 1483–1491)

Lung cancer is the leading cause of cancer death in Japan and is a growing health epidemic worldwide.[1] Moreover, therapies that can cure metastatic LC have not been yet established,[2,3] so there is an urgent need for the development of novel interventions to cure LC.

One of the potential therapeutic targets of NSCLC is STAT3. Constitutively activated STAT3 has been shown to promote tumor cell growth, survival, and tumor angiogenesis, and persistently activated STAT3 has been found in 50% of lung adenocarcinomas.[4] It is thought that STAT3 is activated by JAK, EGFR, or Src family kinases.[5] Among these TYKs, JAK family kinases play an important role in the phosphorylation of STAT3 in NSCLC.[6,7] Dysregulated activation of the JAK/STAT3 signaling pathway, the major downstream pathway of cytokines such as interleukin-6, has been detected in various cancers including NSCLC.[8] Moreover, it has been recently reported that ruxolitinib, which is a potent and selective JAK1 and JAK2 inhibitor, is associated with marked and durable clinical benefits for patients with myelofibrosis, suggesting that JAK kinases are promising therapeutic targets for cancer.[9]

Cytokine signaling pathways are tightly controlled by negative regulatory mechanisms under homeostatic conditions. Suppressors of cytokine signaling family proteins play a role in the negative regulation of cytokine responses by terminating the activation of the JAK/STAT and other signaling pathways.[10–12]

The SOCS family, characterized by a central src homology 2 domain and a conserved C-terminus SOCS box, is composed of eight structurally related proteins.[13] Of these, SOCS-1 is known as the most potent negative regulator of pro-inflammatory cytokine signaling.[14] It interacts with phosphotyrosine residues on proteins such as JAK kinases to interfere with the activation of STAT proteins or other signaling intermediates.[15,16] Also, SOCS-1 recruits the Elongin BC-containing E3 ubiquitin-ligase complex through the conserved SOCS box to promote the degradation of target proteins.[17] Studies of SOCS-1 deficient mice have indicated that SOCS-1 is essential for the inhibition of excessive immune responses and is also involved in the suppression of tumor development.[18,19]

Although it is still not clear whether SOCS shows therapeutic benefit for NSCLC, preclinical analyses of SOCS in therapies of several types of cancers have been carried out worldwide.[20] Previously reported studies by us showed that SOCS-1 or SOCS-3 were effective when used for therapies of malignant pleural mesothelioma or gastric cancer.[21–23] In addition, it has been reported that overexpression of the *SOCS-3* gene showed antitumor effects in NSCLC.[24–26]

In the study presented here, we used the NSCLC cell lines A549, LU65, and PC9 to investigate the possibility of the application of *SOCS-1* gene transduction to NSCLC therapies and the mechanisms of antitumor effects by SOCS-1.

Material and Methods

Cell lines. Both A549 and LU65 cell lines were obtained from the Japanese Collection of Research Bioresources (Osaka, Japan). The PC9 cell line was kindly provided by Prof. Nishio of Kinki University of Medicine, Department of Genome Biology (Osaka, Japan). Details are described in Data S1.

Reagents. PD153035 and JAK inhibitor I were purchased from EMD Millipore (Billerica, MA, USA) and Calbiochem (La Jolla, CA, USA), respectively.

[6]To whom correspondence should be addressed.
E-mail: tnaka@nibio.go.jp

doi: 10.1111/cas.12266

Preparation of adenoviruses. The replication-defective recombinant adenoviral vector expressing the mouse *SOCS-1* gene was provided by Dr. Hiroyuki Mizuguchi (Osaka University, Osaka, Japan), which was constructed with an improved *in vitro* ligation method, as described previously.[27,28] An adenoviral vector expressing the *LacZ* gene was constructed using a similar method and expression of these genes was regulated by means of a CMV promoter/enhancer and intron A. Details are described in Data S1.

Phospho-kinase array. Expression of phosphorylated proteins was detected with the Proteome Profiler Human Phospho-Kinase Array kit (R&D Systems, Minneapolis, MN, USA). Details are described in Data S1.

Cell viability assay. The NSCLC cell lines were plated in 96-well plates at a density of 1×10^3 cells per well and incubated in RPMI-1640 medium containing 10% FCS. Details are described in Data S1.

SDS-PAGE and Western blot analysis. Whole cell protein extracts were prepared from NSCLC cells and tumor tissue in RIPA buffer containing phosphatase inhibitor cocktail and a protease inhibitor cocktail (both from Nacalai Tesque, Kyoto, Japan and both at a concentration of 1×) followed by centrifugation (16 100*g*, 4°C, 15 min). Details are described in Data S1.

Small interfering RNA transfection. Commercial FAK siRNA was obtained from Qiagen (Hilden, Germany). Details are described in Data S1.

Mouse xenograft model. All animal experiments were carried out according to the institutional ethical guidelines for animal experimentation of the National Institute of Biomedical Innovation (Osaka, Japan). Details are described in Data S1.

Immunohistochemistry. Subcutaneously implanted tumors were harvested and paraffin embedded for immunohistochemical analysis using anti-SOCS-1 antibody (Abcam, Cambridge, MA, USA) and anti-Ki-67 antibody (Novocastra Laboratories, Newcastle, UK). A TUNEL assay (with DAPI nuclear counterstaining) for apoptosis was carried out using the ApopTag Fluorescein In Situ Apoptosis Detection Kit (Chemicon International, Temecula, CA, USA) according to the manufacturer's instructions.

Statistical analysis. Data are shown the mean ± SD (unless stated otherwise) for the number of experiments indicated. Details are described in Data S1.

Results

***SOCS-1* gene delivery shows marked antiproliferative effects in A549 and LU65 cells.** We used A549, LU65, and PC9 cell lines, which have been used as NSCLC cell lines in many other experiments. Because the JAK/STAT3 pathway has recently received attention as a novel target for treatment of NSCLC, we investigated the expression levels of JAK family kinases and of STAT3, as well as tyrosine phosphorylation of STAT3 in NSCLC cells. The four known mammalian members of the JAK family are TYK2, JAK1, JAK2, and JAK3. These kinases are widely expressed in a variety of different cell types, with the exception of JAK3, which is selectively expressed in cells of hematopoietic origin.[29] The expression of each JAK was at a similar level in the three cell lines (Fig. 1a). Although phosphorylated STAT3 was detectable in all cell lines, it was markedly more elevated in A549 and LU65 (Fig. 1b).

We next investigated whether SOCS-1 could suppress proliferation of A549, LU65, and PC9. Following *SOCS-1* gene delivery, overexpression of SOCS-1 was detected in all cell lines by Western blot analysis (Fig. 1c), but overexpression of SOCS-1 had antiproliferative effects on A549 and LU65 but not on PC9 (Fig. 1d).

Overexpression of SOCS-1 shows stronger antiproliferative effect than JAK inhibitor in NSCLC cells. Immunoblotting analysis showed that the expression levels of some of the JAK family kinases in all cell lines were reduced by overexpression of SOCS-1 (Fig. 2a). Next, phosphorylation levels of STAT3 (Tyr705), a downstream molecule of the JAK kinase family, were analyzed by Western blot analysis. Phosphorylation levels of STAT3 (Tyr705) were decreased in response to overexpression of the *SOCS-1* gene in all cell lines (Fig. 2b). These results agree with previously reported findings that SOCS-1 can act directly on JAK family kinases to suppress their kinase activity as well as to accelerate their degradation by the recruitment of an E3 ubiquitin ligase.[17]

Although the JAK/STAT3 pathway was downregulated by SOCS-1 in all cell lines, overexpression of the *SOCS-1* gene showed an antiproliferative effect only on A549 and LU65 cells. Accordingly, we next used JAK inhibitor I, a blocker of JAK1, JAK2, and JAK3, instead of AdSOCS-1 to examine the effects of JAK inhibition on all cell lines. Proliferation of A549 and LU65 cells was significantly suppressed by treatment with JAK inhibitor I, however, proliferation of PC9 was not significantly suppressed (Fig. 2c). Immunoblotting analysis showed that tyrosine phosphorylation of STAT3 was downregulated in all cell lines after introduction of JAK inhibitor I (Fig. 2d). These findings suggest that JAK-mediated signals are critical for the proliferation of A549 and LU65 cells, but are not needed for that of PC9 cells. In addition, because JAK1 and JAK2 are overlapping target molecules between SOCS-1 and JAK inhibitor I, the primary target molecules of SOCS-1 in NSCLC cells are likely to be JAK1 and/or JAK2. Therefore, we assumed that the antiproliferative effect of SOCS-1 was essentially determined by the JAK-dependence of NSCLC cells.

Immunoblotting analysis showed that introduction of both the *SOCS-1* gene (at 40 MOI) and of JAK inhibitor I (5 μM) could effectively suppress STAT3 phosphorylation (Fig. 2b,d). However, SOCS-1 was more effective than JAK inhibitor I for inhibiting proliferation of A549 and LU65 cells (Fig. 2e). Because SOCS-1 is known as an adaptor of several molecules other than JAK family kinases,[19] it was expected that AdSOCS-1 could also exert JAK-independent action in A549 and LU65. To investigate in detail the mechanisms of antitumor effects induced by overexpression of SOCS-1, we used A549 cells for further analyses.

Focal adhesion kinase is downregulated by overexpression of SOCS-1 in A549. Focal adhesion kinase is known as an adhesion molecule and previous investigations have indicated that FAK contributes to tumor cell proliferation, survival, and metastasis.[30] SOCS-1 was found to inhibit FAK-dependent signaling events by suppressing FAK-associated kinase activity and tyrosine phosphorylation of FAK,[31] and also by promoting polyubiquitination and degradation of FAK in a SOCS box-dependent manner.[17] For this reason, we next focused on the FAK pathway and examined the levels of FAK expression and of FAK tyrosine phosphorylation after overexpression of the *SOCS-1* gene.

Focal adhesion kinase expression was upregulated by introduction of the *LacZ* gene in A549 cells (Fig. 3a), probably reflecting the previously reported non-specific stimulation by adenovirus vectors.[32] Compared to the cells introduced by *LacZ*, FAK phosphorylation (Tyr397) was downregulated after the introduction of the *SOCS-1* gene in A549 (Fig. 3a). We also investigated whether JAK inhibitor I, instead of SOCS-1, can suppress activation of FAK in A549 cells, and found that JAK inhibitor could not (Fig. 3b).

We assumed that downregulation of FAK by SOCS-1 could contribute to the inhibition of A549 cell proliferation. Therefore, examined whether FAK siRNA indeed had an antiproliferative effect on A549, and found that proliferation of A549 cells was suppressed by FAK knockdown, indicating that these cells are dependent on FAK (Fig. 3c,d). We also investigated

doi: 10.1111/cas.12266

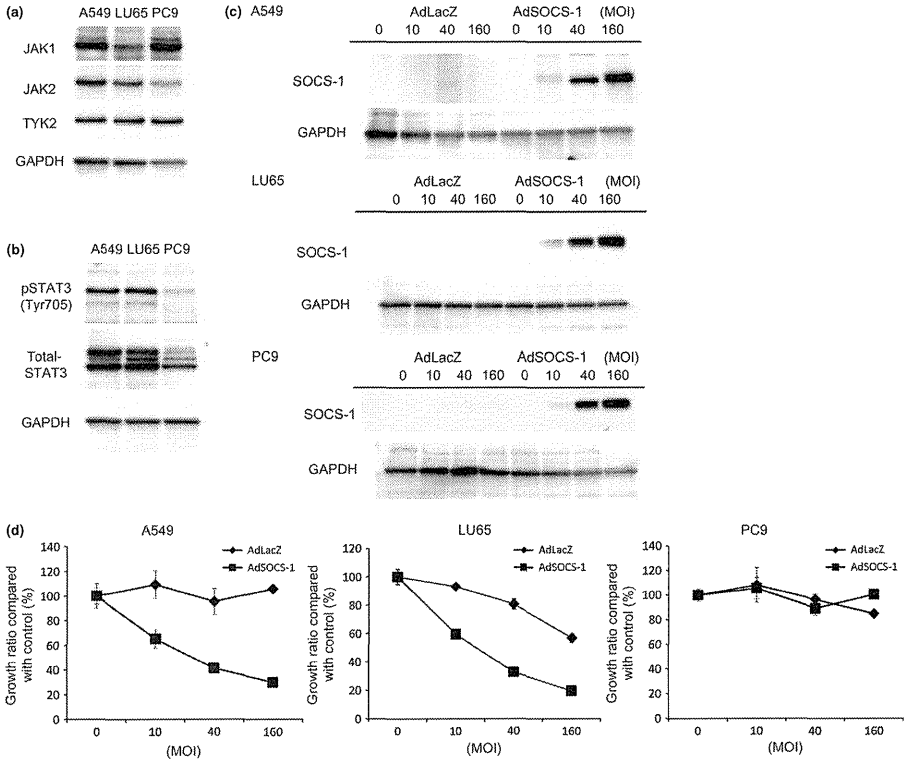

Fig. 1. Delivery of *SOCS-1* gene shows marked antiproliferative effects in A549 and LU65 lung cancer cell lines. (a) Expression of JAK family kinases in all cell lines determined by Western blotting. Cell lysates were immunoblotted with JAK1, JAK2, or tyrosine kinase 2 (TYK2) antibodies. (b) Comparative analysis of phosphorylation and expression of signal transducer and activator of transcription 3 (STAT3) determined by Western blotting. (c) Cell lysates were prepared 48 h after treatment with AdSOCS-1or AdLacZ adenoviral vectors at an MOI of 10–160, and immunoblotted with anti-SOCS-1 antibody. (d) Cells were infected with AdSOCS-1 or AdLacZ at an MOI of 10–160. Cell proliferation was determined by MTS assay 72 h after transfection. Growth ratio of AdLacZ or AdSOCS-1-infected cells was calculated by a percentage of that for non-treated cells. Each value represents the average ± SD of hexaplicate wells.

the combined effect of JAK inhibitor I and FAK siRNA on A549 cell proliferation. The results showed that the combined effect was stronger than that of JAK inhibitor I alone (Fig. 3e). These findings suggest that FAK has an important role in A549 cell proliferation independent of JAK and that SOCS-1-mediated FAK inhibition might contribute to the suppression of proliferation of A549 cells treated with AdSOCS-1.

Epidermal growth factor receptor is downregulated by overexpression of SOCS-1 in A549. Expression of *SOCS-1* reportedly interacts with the cytoplasmic domain of EGFR and is likely to induce ubiquitination and degradation of ligand-bound EGFR.[33] This notion was confirmed by means of immunoblotting analysis in our study, in that EGFR expression was downregulated 48 h after introduction of the *SOCS-1* gene in A549 cells. The EGFR phosphorylation (Tyr1068) was also downregulated after overexpression of the *SOCS-1* gene had occurred in A549 cells (Fig. 4a). In contrast, JAK inhibitor I did not suppress EGFR activation in A549 cells (Fig. 4b).

We next examined the antiproliferative effects of the EGFR inhibitor PD153035 on A549 cells. Expression of EGFR in A549 cells was much lower than that in PC9 cells (data not shown), which harbor a deletion of an EGFR mutation.[34] Nevertheless, our findings show that proliferation of A549 cells with wild-type EGFR were also somewhat dependent on EGFR (Fig. 4c,d). We also investigated the combined effect of JAK inhibitor I and PD153035 on proliferation of A549 cells and found that they have an additive effect (Fig. 4e). This finding suggests that EGFR is also involved in A549 cell proliferation independent of JAK and that its downregulation by SOCS-1 may have an inhibitory effect on proliferation of A549 cells.

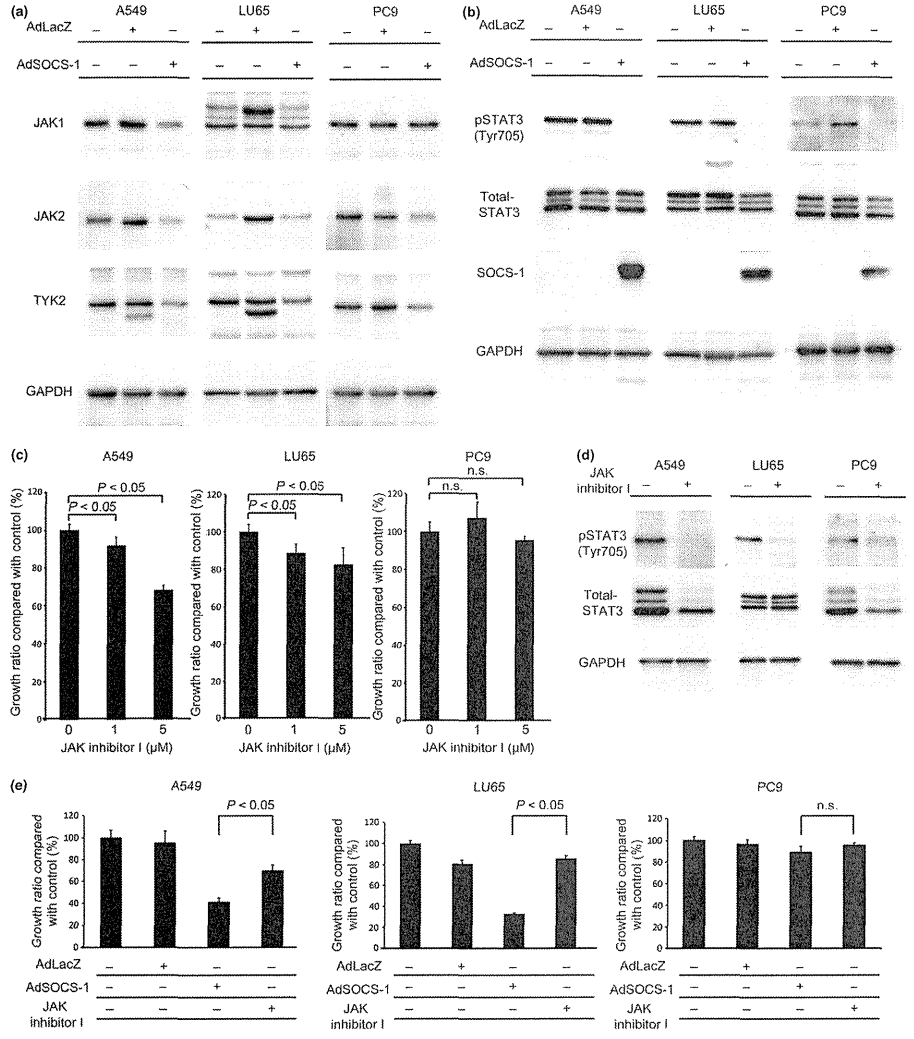

Fig. 2. Antiproliferative effect of suppressor of cytokine signaling-1 (SOCS-1) correlated with JAK dependence is stronger than JAK inhibitor. (a) Cell lysates were prepared 48 h after treatment with AdSOCS-1 or AdLacZ adenoviral vectors at an MOI of 40 and immunoblotted with JAK1, JAK2, or tyrosine kinase 2 (TYK2) antibodies. (b) SOCS-1 suppressed activation of signal transducer and activator of transcription 3 (STAT3). Cell lysates were prepared as described above and immunoblotted with anti-p-STAT3 (Tyr705), anti-STAT3, and anti-SOCS-1 antibodies. (c) Cells cultured in RPMI-1640 medium containing 10% FBS were exposed to 1–5 μM JAK inhibitor I. After incubation for 72 h, viable cells were counted with the MTS assay. (d) Cells were cultured in RPMI-1640 medium containing 0.5% FBS with 5 μM JAK inhibitor I. Cell lysates were immunoblotted with anti-p-STAT3 (Tyr705) and anti-STAT3 antibodies. (e) All cell lines cultured in RPMI-1640 medium containing 10% FBS were exposed to 5 μM JAK inhibitor I, or infected with AdLacZ or AdSOCS-1 at an MOI of 40. After incubation for 72 h, viable cells were counted with the MTS assay.

doi: 10.1111/cas.12266

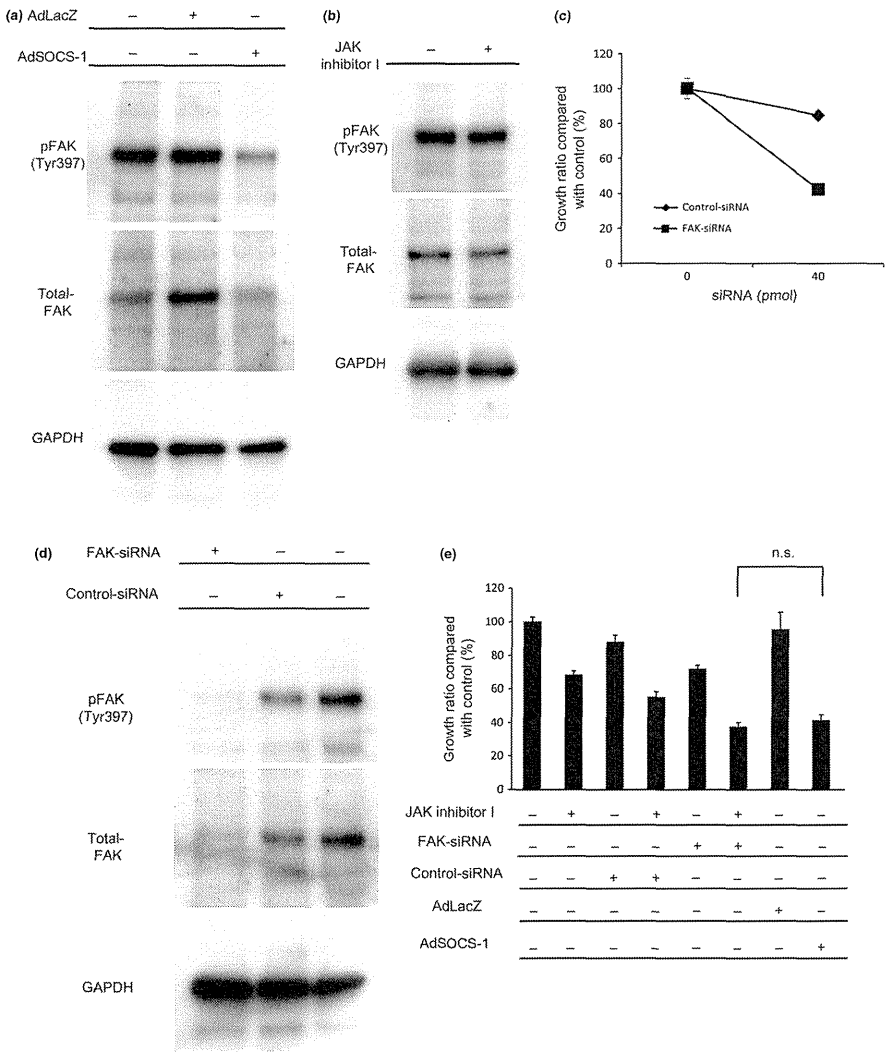

Fig. 3. Focal adhesion kinase (FAK) is downregulated by adenovirus vector containing suppressor of cytokine signaling-1 (AdSOCS-1) in A549 lung cancer cells. (a) Cell lysates were prepared 48 h after treatment with AdSOCS-1 or AdLacZ at an MOI of 40, and immunoblotted with p-FAK (Tyr397) and FAK antibodies. (b) Cell lysates were prepared 48 h after exposure to 5 μM JAK inhibitor I and immunoblotted with p-FAK (Tyr397) and FAK antibodies. (c) Cells were exposed to either FAK siRNA or non-specific siRNA as control. Cells were cultured in RPMI-1640 medium containing 10% FBS. After a 3-day culture, viable cells were counted with the MTS assay. (d) Protein extracts prepared at 48 h after treatment with FAK siRNA or non-specific siRNA were blotted with anti-p-FAK (Tyr397) and anti-FAK antibodies. (e) A549 cells cultured in RPMI-1640 medium containing 10% FBS were exposed to 5 μM JAK inhibitor I or 40 pmol FAK siRNA; 40 pmol non-specific siRNA was used as control. Infections of AdLacZ or AdSOCS-1 were carried out at an MOI of 40. Cell proliferation activity was assessed by MTS assay 72 h after treatment. n.s., no significant change detected by Tukey's post-hoc comparisons.

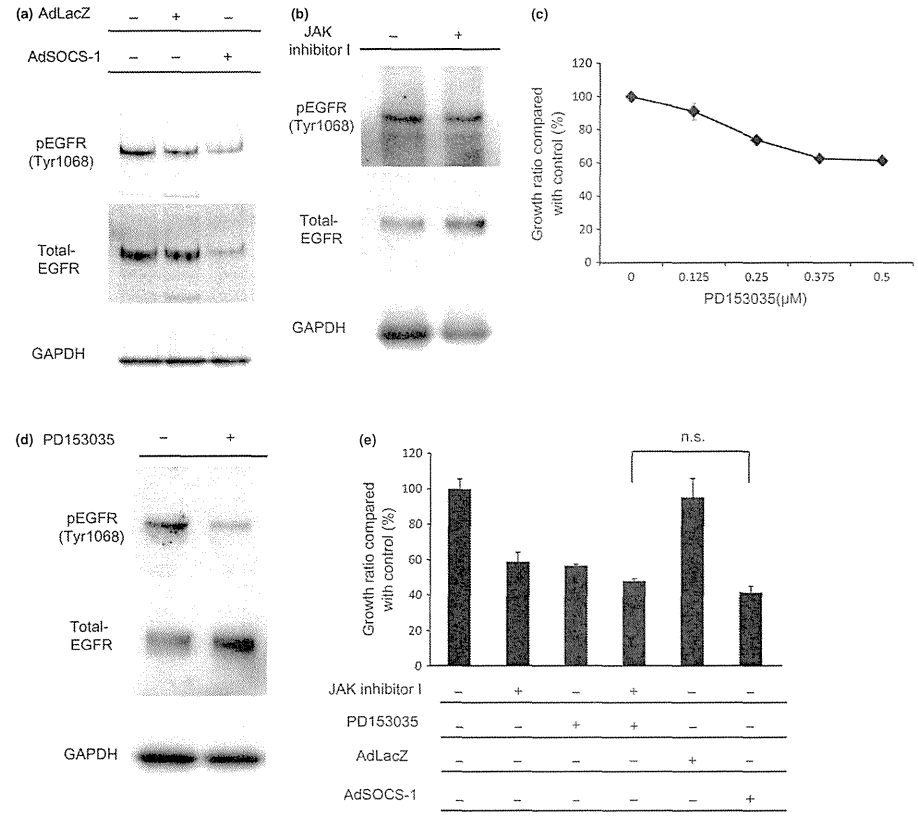

Fig. 4. Epidermal growth factor receptor (EGFR) is downregulated by adenovirus vector containing suppressor of cytokine signaling-1 (AdSOCS-1) in A549 lung cancer cells. (a) Cells were infected with AdLacZ or AdSOCS-1 at an MOI of 40 for 24 h. Cell lysates were immunoblotted with anti-p-EGFR (Tyr1068) and anti-EGFR antibodies. (b) Cell lysates were prepared 48 h after exposure to 5 μM JAK inhibitor I and immunoblotted with anti-p-EGFR (Tyr1068) and anti-EGFR antibodies. (c) Cells cultured in RPMI-1640 medium containing 10% FBS were exposed to 0.125–0.5 μM PD153035. Cell proliferation activity was assessed by MTS assay 72 h after exposure. (d) A549 cells were cultured in RPMI-1640 medium containing 0.5% FBS with 0.5 μM PD153035. Cell lysates were prepared 48 h after treatment and immunoblotted with anti-p-EGFR (Tyr1068) and anti-EGFR antibodies. (e) A549 cells cultured in RPMI-1640 medium containing 10% FBS were exposed to 5 μM JAK inhibitor I or 0.5 μM PD153035. Infection of AdLacZ or AdSOCS-1 was carried out at an MOI of 40. Cell proliferation activity was assessed by MTS assay 72 h after treatment. n.s., no significant change detected by Tukey's post-hoc comparisons.

Accordingly, JAK1, JAK2, FAK, and EGFR should be considered critical for the proliferation of A549 cells, so that simultaneous inhibition of these molecules by SOCS-1 may have a potent antiproliferative effect on A549.

Upregulation of p53 by AdSOCS-1 in A549 cells. We also used a phospho-kinase array to determine the expression profile of phosphorylated proteins in A549 in order to identify other target molecules for SOCS-1 in addition to JAK, FAK, and EGFR (Fig. 5a). Phosphorylation of p53 was upregulated in A549 cells after the introduction of the *SOCS-1* gene. This was confirmed by immunoblotting analysis, which showed that p53 phosphorylation was upregulated in A549 cells by overexpression of the *SOCS-1* gene (Fig. 5b). We also investigated whether JAK inhibitor I, instead of SOCS-1, could activate p53 in A549 cells, but found that it did not (Fig. 5b). Given the well-established antitumor effect of p53 phoshorylation,[35,38] SOCS-1-induced p53 activation may thus also contribute to the suppression of A549 cell proliferation.

Antitumor activity of *SOCS-1* in a lung cancer xenograft model. We also evaluated the therapeutic effect of AdSOCS-1 injection on the growth of NSCLC cells *in vivo*. We established a xenograft model of ICR nu/nu mice in which A549 cells were s.c. implanted. Injection of AdSOCS-1 vector

doi: 10.1111/cas.12266

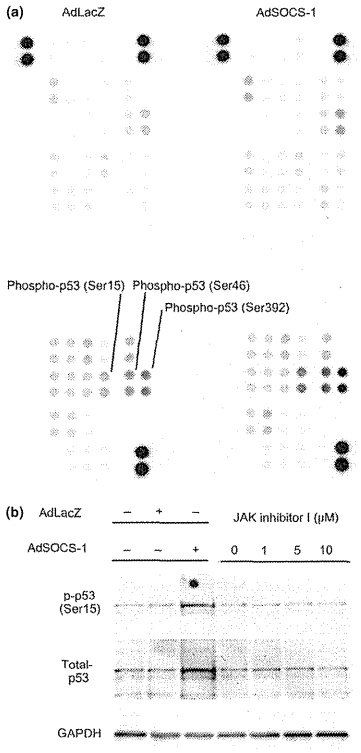

Fig. 5. Protein p53 is upregulated by adenovirus vector containing suppressor of cytokine signaling-1 (AdSOCS-1) in A549 lung cancer cells. (a) A549 cells were cultured in RPMI-1640 medium containing 10% FBS with AdSOCS-1 at an MOI of 40. After a 24-h culture, protein extracts were examined with a phospho-kinase array with each phosphorylated protein identified in duplicate. The double-labeled spots in the upper right corner represent the positive controls. (b) Cell lysates were prepared 48 h after infection with AdLacZ or AdSOCS-1 at an MOI of 40. Cell lysates were immunoblotted with anti-phospho-53 (p-p53 [Ser15]) and anti-p53 antibodies. (c) Cell lysates were prepared 48 h after exposure to 5 μM JAK inhibitor I and immunoblotted with anti-p-p53 (Ser15) and anti-p53 antibodies.

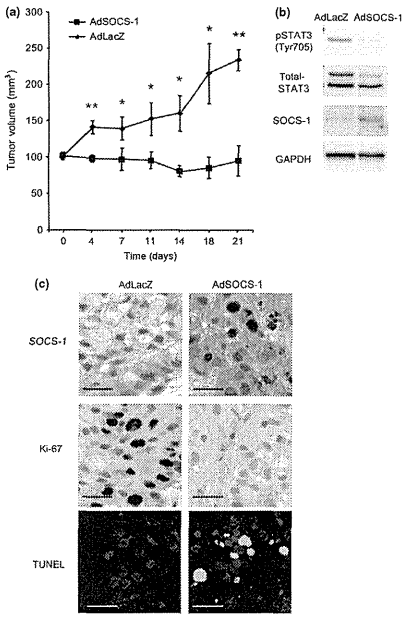

Fig. 6. Suppressor of cytokine signaling-1 (SOCS-1) shows antitumor activity in a lung cancer xenograft model. (a) Female ICR nu/nu mice were s.c. implanted with 2×10^6 A549 cells in their flank. When the calculated tumor volumes reached to approximately 100 mm^3, 4×10^8 pfu AdSOCS1 or AdLacZ adenoviral vectors were intratumorally treated twice per week. Tumor volumes were determined twice per week. The mean volume ± SEM of five tumors in each group, and were analyzed by Student's *t*-test (*$P < 0.05$, **$P < 0.01$). (b) Western blot analysis of phosphorylated signal transducer and activator of transcription 3 (pSTAT3), STAT3, SOCS-1, and GAPDH in A549 tissues from AdSOCS-1 or AdLacZ injected animals. Lysates from tumors were analyzed by Western blotting. (c) Immunohistochemical analysis of SOCS-1, Ki-67, and TUNEL (blue fluorescence, DAPI staining for nuclei; cyan fluorescence, TUNEL positivity) in A549 tissues from animals injected with AdSOCS-1 or AdLacZ. Scale bar = 25 μm.

(4×10^8 pfu) intratumorally twice per week significantly suppressed tumor growth compared to control AdLacZ injection (Fig. 6a). AdSOCS-1 *in vivo* could modulate intracellular signaling in NSCLC cells as *in vitro*, as Western blot analysis showed that phosphorylation levels of STAT3 were decreased in the A549 tissues from AdSOCS-1 injected animals (Fig. 6b). Furthermore, few Ki-67-positive nuclei were detected by immunohistochemical analysis in AdSOCS-1 infected tissues compared to AdLacZ, indicating that proliferating cells are decreased by overexpression of SOCS-1 (Fig. 6c). Additionally, induction of apoptosis was detected in AdSOCS-1 infected A549 tissue compared to AdLacZ by TUNEL analysis (Fig. 6c).

Discussion

In this study, we investigated the possibility that SOCS-1 could be used in LC therapies. Previous reports showed that PC9 harbors a deletion mutation in EGFR and that A549 and LU65 cells possess wild-type EGFR.[34,39] Although EGFR mutation in NSCLC was previously reported to activate AKT, MAPK, and STAT3 signaling,[40] our research showed that STAT3 was more strongly expressed in A549 and LU65 than in PC9 cells, and that sensitivity to overexpression of SOCS-1 was also higher in A549 and LU65 cells than in PC9 (Fig. 1). In addition, JAK inhibitor I significantly suppressed proliferation of A549 and LU65 cells, but not of PC9. Therefore, we consider that the marked antiproliferative effect by overexpression of SOCS-1 on A549 and LU65 cells, but not on PC9, was attributable to the inhibition of JAK/STAT3 pathway *in vitro*. As SOCS-1 also shows an antiproliferative effect *in vivo* (Fig. 6), AdSOCS1 gene therapy might be effective for patients with NSCLC, in which the JAK/STAT3 signaling pathway is constitutively activated. It has been reported that approximately 50% of NSCLC tumors showed elevated phosphorylation levels of STAT3 (Tyr705) by immunohistochemical analysis.[4] There is a further possibility that LC patients harboring STAT3 dependence, detected by immunostaining analysis of phosphorylation levels of STAT3 (Tyr705) in specimens obtained surgically or bronchoscopically, could be selected for treatment with SOCS-1 overexpression.

Comparative analyses of the antiproliferative effects of *SOCS-1* gene introduction and JAK inhibitor I treatment suggest that overexpression of SOCS-1 may have a stronger effect than that of the JAK inhibitor I on A549 and LU65 cells (Fig. 2e). In fact, SOCS-1, but not JAK inhibitor I, inhibited FAK and EGFR, which are important for the survival of A549 cells. In addition, the combined effect of FAK siRNA and JAK inhibitor I, or that of PD153035 and JAK inhibitor I, was superior to the antiproliferative effect of JAK inhibitor alone (Figs 3,4). These findings suggest that the potent antiproliferative effect of SOCS-1 depends not only on JAK inhibition but also on the suppression of other distinct signal transduction pathways, such as FAK and EGFR. In addition, phosphorylation of p53 at Ser15 was enhanced by the overexpression of the *SOCS-1* gene in A549 cells (Fig. 5). Because phosphorylation of p53 at Ser15 contributes to antitumor effects under certain experimental conditions,[35–38] and A549 cells express wild-type p53,[41] activation of p53 by SOCS-1 overexpression seems to be involved in the antitumor effects.[42]

In conclusion, the findings of our study suggest that *SOCS-1* gene therapy is potentially effective for at least a subset of NSCLC both *in vitro* and *in vivo*. It was shown that SOCS-1 had a potent antiproliferative effect on JAK-dependent NSCLC cells by targeting the JAK/STAT3 pathway. In addition, SOCS-1 successfully targeted many factors such as FAK, EGFR, and p53 in NSCLC cells. It is thus possible that *SOCS-1* gene therapy could have a unique advantage over JAK inhibitor for the treatment of NSCLC.

Further studies will be needed to elucidate the mechanism of JAK/STAT3 pathway-dependence in NSCLC, and to validate the benefits that *SOCS-1* gene therapy could provide for NSCLC treatment in clinical practice.

Acknowledgments

This work was supported by a Grant-in-Aid from the Ministry of Health, Labour and Welfare, Japan (T. Naka) and a grant from the Kansai Biomedical Cluster Project in Saito, which is promoted by the Knowledge Cluster Initiative of the Ministry of Education, Culture, Sports, Science and Technology, Japan (T. Naka). The authors are grateful to Ms. M. Urase for experimental assistance and Ms. Y. Kanazawa and Ms. J. Yamagishi for secretarial assistance.

Disclosure Statement

The authors have no conflict of interest.

Abbreviations

AdSOCS-1	adenovirus vector containing SOCS-1
EGFR	epidermal growth factor receptor
FAK	focal adhesion kinase
LC	lung cancer
NSCLC	non-small-cell lung cancer
SOCS	suppressor of cytokine signaling
STAT	signal transducer and activator of transcription
TYK	tyrosine kinase

References

1 Hattori M, Fujita M, Ito Y, Ioka A, Katanoda K, Nakamura Y. Use of a population-based cancer registry to calculate twenty-year trends in cancer incidence and mortality in Fukui Prefecture. *J Epidemiol* 2010; **20**: 244–52.
2 Goffin J, Lacchetti C, Ellis PM, Ung YC, Evans WK. First-line systemic chemotherapy in the treatment of advanced non-small cell lung cancer: a systematic review. *J Thorac Oncol* 2010; **5**: 260–74.
3 Rossi A, Di Maio M, Chiodini P *et al.* Carboplatin- or cisplatin-based chemotherapy in first-line treatment of small-cell lung cancer: the COCIS meta-analysis of individual patient data. *J Clin Oncol* 2012; **30**: 1692–8.
4 Gao SP, Mark KG, Leslie K *et al.* Mutations in the EGFR kinase domain mediate STAT3 activation via IL-6 production in human lung adenocarcinomas. *J Clin Invest* 2007; **117**: 3846–56.
5 Lai SY, Johnson FM. Defining the role of the JAK-STAT pathway in head and neck and thoracic malignancies: implications for future therapeutic approaches. *Drug Resist Updat* 2010; **13**: 67–78.
6 Song L, Rawal B, Nemeth JA, Haura EB. JAK1 activates STAT3 activity in non-small-cell lung cancer cells and IL-6 neutralizing antibodies can suppress JAK1-STAT3 signaling. *Mol Cancer Ther* 2011; **10**: 481–94.
7 Guo Y, Xu F, Lu T, Duan Z, Zhang Z. Interleukin-6 signaling pathway in targeted therapy for cancer. *Cancer Treat Rev* 2012; **38**: 904–10.
8 Jiang R, Jin Z, Liu Z, Sun L, Wang L, Li K. Correlation of activated STAT3 expression with clinicopathologic features in lung adenocarcinoma and squamous cell carcinoma. *Mol Diagn Ther* 2011; **15**: 347–52.
9 Verstovsek S, Kantarjian H, Mesa RA *et al.* Safety and efficacy of INCB018424, a JAK1 and JAK2 inhibitor, in myelofibrosis. *N Engl J Med* 2010; **363**: 1117–27.
10 Naka T, Narazaki M, Hirata M *et al.* Structure and function of a new STAT-induced STAT inhibitor. *Nature* 1997; **387**: 924–9.
11 Starr R, Willson TA, Viney EM *et al.* A family of cytokine-inducible inhibitors of signalling. *Nature* 1997; **387**: 917–21.
12 Endo TA, Masuhara M, Yokouchi M *et al.* A new protein containing an SH2 domain that inhibits JAK kinases. *Nature* 1997; **387**: 921–4.
13 Piessevaux J, Lavens D, Peelman F, Tavernier J. The many faces of the SOCS box. *Cytokine Growth Factor Rev* 2008; **19**: 371–81.
14 Yoshimura A, Suzuki M, Sakaguchi R, Hanada T, Yasukawa H. SOCS, Inflammation, and Autoimmunity. *Front Immunol* 2012; **3**: 20.
15 Narazaki M, Fujimoto M, Matsumoto T *et al.* Three distinct domains of SSI-1/SOCS-1/JAB protein are required for its suppression of interleukin 6 signaling. *Proc Natl Acad Sci USA* 1998; **95**: 13130–4.
16 Yasukawa H, Misawa H, Sakamoto H *et al.* The JAK-binding protein JAB inhibits Janus tyrosine kinase activity through binding in the activation loop. *EMBO J* 1999; **18**: 1309–20.
17 Valentino L, Pierre J. JAK/STAT signal transduction: regulators and implication in hematological malignancies. *Biochem Pharmacol* 2006; **71**: 713–21.
18 Naka T, Fujimoto M, Tsutsui H, Yoshimura A. Negative regulation of cytokine and TLR signalings by SOCS and others. *Adv Immunol* 2005; **87**: 61–122.
19 Yoshimura A, Naka T, Kubo M. SOCS proteins, cytokine signalling and immune regulation. *Nat Rev Immunol* 2007; **7**: 454–65.
20 Zhang J, Li H, Yu JP, Wang SE, Ren XB. Role of SOCS1 in tumor progression and therapeutic application. *Int J Cancer* 2012; **130**: 1971–80.
21 Iwahori K, Serada S, Fujimoto M *et al.* Overexpression of SOCS3 exhibits preclinical antitumor activity against malignant pleural mesothelioma. *Int J Cancer* 2011; **129**: 1005–17.
22 Souma Y, Nishida T, Serada S *et al.* Antiproliferative effect of SOCS-1 through the suppression of STAT3 and p38 MAPK activation in gastric cancer cells. *Int J Cancer* 2012; **131**: 1287–96.
23 Iwahori K, Serada S, Fujimoto M *et al.* SOCS-1 gene delivery cooperates with cisplatin plus pemetrexed to exhibit preclinical antitumor activity against malignant pleural mesothelioma. *Int J Cancer* 2013; **132**: 459–71.
24 Baltayiannis G, Baltayiannis N, Tsianos EV. Suppressors of cytokine signaling as tumor repressors. Silencing of SOCS3 facilitates tumor formation and growth in lung and liver. *J BUON* 2008; **13**: 263–5.
25 Zhang S, Guo D, Jiang L, Zhang Q, Qiu X, Wang E. SOCS3 inhibiting migration of A549 cells correlates with PYK2 signaling in vitro. *BMC Cancer* 2008; **8**: 150.

doi: 10.1111/cas.12266

26 Lin YC, Lin CK, Tsai YH *et al.* Adenovirus-mediated SOCS3 gene transfer *inhibits the growth and enhances the radiosensitivity of human non-small* cell lung cancer cells. *Oncol Rep* 2010; **24**: 1605–12.
27 Mizuguchi H, Kay MA. A simple method for constructing E1- and E1/E4-deleted recombinant adenoviral vectors. *Hum Gene Ther* 1999; **10**: 2013–7.
28 Sakurai H, Tashiro K, Kawabata K *et al.* Adenoviral expression of suppressor of cytokine signaling-1 reduces adenovirus vector-induced innate immune responses. *J Immunol* 2008; **180**: 4931–8.
29 Verma A, Kambhampati S, Parmar S, Platanias LC. Jak family of kinases in cancer. *Cancer Metastasis Rev* 2003; **22**: 423–34.
30 Schmidmaier R, Baumann P. ANTI-ADHESION evolves to a promising therapeutic concept in oncology. *Curr Med Chem* 2008; **15**: 978–90.
31 Liu E, Cote JF, Vuori K. Negative regulation of FAK signaling by SOCS proteins. *EMBO J* 2003; **22**: 5036–46.
32 Kornberg LJ, Grant MB. Adenoviruses increase endothelial cell proliferation, migration, and tube formation: partial reversal by the focal adhesion kinase inhibitor, FRNK. *Microvasc Res* 2007; **73**: 157–62.
33 Quesnelle KM, Boehm AL, Grandis JR. STAT-mediated EGFR signaling in cancer. *J Cell Biochem* 2007; **102**: 311–9.
34 Zhang D, Takigawa N, Ochi N *et al.* Detection of the EGFR mutation in exhaled breath condensate from a heavy smoker with squamous cell carcinoma of the lung. *Lung Cancer* 2011; **73**: 379–80.
35 Lai JM, Chang JT, Wen CL, Hsu SL. Emodin induces a reactive oxygen species-dependent and ATM-p53-Bax mediated cytotoxicity in lung cancer cells. *Eur J Pharmacol* 2009; **623**: 1–9.
36 Amin AR, Wang D, Zhang H *et al.* Enhanced anti-tumor activity by the *combination of the natural compounds (-)-epigallocatechin-3-gallate and* luteolin: potential role of p53. *J Biol Chem* 2010; **285**: 34557–65.
37 Oh HL, Lee DK, Lim H, Lee CH. HY253, a novel decahydrofluorene analog, from Aralia continentalis, induces cell cycle arrest at the G1 phase and cytochrome c-mediated apoptosis in human lung cancer A549 cells. *J Ethnopharmacol* 2010; **129**: 135–9.
38 Yamada C, Ozaki T, Ando K *et al.* RUNX3 modulates DNA damage-mediated phosphorylation of tumor suppressor p53 at Ser-15 and acts as a co-activator for p53. *J Biol Chem* 2010; **285**: 16693–703.
39 Nagai Y, Miyazawa H, Huqun *et al.* Genetic heterogeneity of the epidermal growth factor receptor in non-small cell lung cancer cell lines revealed by a rapid and sensitive detection system, the peptide nucleic acid-locked nucleic acid PCR clamp. *Cancer Res* 2005; **65**: 7276–82.
40 Zimmer S, Kahl P, Buhl TM *et al.* Epidermal growth factor receptor mutations in non-small cell lung cancer influence downstream Akt, MAPK and Stat3 signaling. *J Cancer Res Clin Oncol* 2009; **135**: 723–30.
41 Kashii T, Mizushima Y, Monno S, Nakagawa K, Kobayashi M. Gene analysis of K-, H-ras, p53, and retinoblastoma susceptibility genes in human lung cancer cell lines by the polymerase chain reaction/single-strand conformation polymorphism method. *J Cancer Res Clin Oncol* 1994; **120**: 143–8.
42 Mallette FA, Calabrese V, Ilangumaran S, Ferbeyre G. SOCS1, a novel interaction partner of p53 controlling oncogene-induced senescence. *Aging (Albany NY)* 2010; **2**: 445–52.

Supporting Information

Additional supporting information may be found in the online version of this article:

Data S1. Methods.

IJC
International Journal of Cancer

New findings of kinase switching in gastrointestinal stromal tumor under imatinib using phosphoproteomic analysis

Tsuyoshi Takahashi[1,2], Satoshi Serada[2], Maiko Ako[2], Minoru Fujimoto[2], Yasuaki Miyazaki[1], Rie Nakatsuka[1,2], Takayuki Ikezoe[3], Akihito Yokoyama[3], Takahiro Taguchi[4], Kazuki Shimada[5], Yukinori Kurokawa[1], Makoto Yamasaki[1], Hiroshi Miyata[1], Kiyokazu Nakajima[1], Shuji Takiguchi[1], Masaki Mori[1], Yuichiro Doki[1], Tetsuji Naka[2] and Toshirou Nishida[2,6]

[1] Department of Surgery, Osaka University Graduate School of Medicine, Suita, Japan
[2] Laboratory for Immune Signal, National Institute of Biomedical Innovation, Ibaraki, Japan
[3] Department of Hematology and Respiratory Medicine, Kochi Medical School, Kochi University, Nankoku, Japan
[4] Research and Education Faculty, Multidisciplinary Science Cluster, Kuroshio Science Unit, Kochi Medical School, Kochi University, Nankoku, Japan
[5] Department of Respiratory Medicine, Allergy and Rheumatic Diseases, Osaka University Graduate School of Medicine, Suita, Japan
[6] Department of Surgery, Osaka Police Hospital, Osaka, Japan

Despite the revolutionary effects of imatinib on advanced gastrointestinal stromal tumors (GISTs), most patients eventually develop disease progression following primary resistance or acquired resistance driven by secondary-resistant mutations. Even in radiographically vanishing lesions, pathology has revealed persistent viable cells during imatinib therapy, which could lead to the emergence of drug-resistant clones. To uncover the mechanisms underlying these clinical issues, here we examined imatinib-induced phosphoproteomic alterations in GIST-T1 cells, using our quantitative tyrosine phosphoproteomic analysis method, which combined immunoaffinity enrichment of phosphotyrosine-containing peptides with isobaric tags for relative and absolute quantitation (iTRAQ) technology. Using this approach, we identified 171 tyrosine phosphorylation sites spanning 134 proteins, with 11 proteins exhibiting greater than 1.5-fold increases in tyrosine phosphorylation. Among them, we evaluated FYN and focal adhesion kinase (FAK), both of which are reportedly involved in proliferation and malignant alteration of tumors. We confirmed increased tyrosine phosphorylation of both kinases by western blotting. Inhibition of FYN and FAK phosphorylation each increased tumor cell sensitivity to imatinib. Furthermore, a FAK-selective inhibitor (TAG372) induced apoptosis of imatinib-resistant GIST-T1 cells and decreased the imatinib IC_{50}. These results indicate that FYN or FAK might be potential therapeutic targets to overcome resistance to imatinib in GISTs. Additionally, we showed that the iTRAQ-based quantitative phosphotyrosine-focused phosphoproteomic approach is a powerful method for screening phosphoproteins associated with drug resistance.

The gastrointestinal stromal tumor (GIST) is the most common mesenchymal tumor of the digestive tract, and is characterized by expression of the KIT (CD117) and/or DOG1 proteins. Most GISTs have oncogenic *KIT* or *PDFGRA* mutations, which is a key factor in sporadic GIST pathogenesis and proliferation.[1–3] This knowledge has facilitated the development of targeted therapies with tyrosine kinase inhibitors and led to the revolutionary treatment with imatinib mesylate (Glivec®; Novartis Pharmaceuticals). Recent clinical trials with advanced/unresectable GIST have shown that imatinib produces objective responses in ~50% of patients, and disease stabilization (stable disease) in another 30–40%. The corresponding 2-year overall survival rates range from 70 to 80%, indicating markedly improved patient outcomes compared with anecdotal data from cytotoxic chemotherapy in the preimatinib era.[4–6]

Despite imatinib's effectiveness, there remain several problems. First, GIST patients cannot stop taking the drug even if complete response is obtained, because discontinuation inevitably leads to reprogression and disease relapse.[7,8] Second, imatinib activity is limited by primary resistance to the drug in ~15% of patients, and secondary resistance eventually develops in more than 80% of patients.[5,9] Secondary resistance mainly occurs due to additional kinase domain mutations, which are thought to develop in viable tumor cells (persistent cells) during imatinib therapy. It is not yet known

Key words: GIST, imatinib, iTRAQ, proteomics
Abbreviations: FAK: focal adhesion kinase; GIST: gastrointestinal stromal tumor; iTRAQ: isobaric tags for relative and absolute quantitation; LC: liquid chromatography; MS/MS: tandem mass spectrometry; shRNA: small hairpin RNA; siRNA: small interfering RNA
Additional Supporting Information may be found in the online version of this article.
DOI: 10.1002/ijc.28282
History: Received 17 Dec 2012; Accepted 2 May 2013; Online 28 May 2013

Correspondence to: Toshirou Nishida, Department of Surgery, Osaka Police Hospital, 10-31, Kitayama-cho, Tennoji-ku, Osaka 543-0035, Japan, Tel.: +81-6-6771-6051, Fax: +81-6-6775-2838, E-mail: toshin@mvb.biglobe.ne.jp

Short Report

What's new?

While the targeted tyrosine kinase inhibitor imatinib can significantly improve two-year survival rates for patients with gastrointestinal stromal tumor (GIST), primary and secondary resistance mutations often limit its benefits. This study of the human GIST-T1 cell line suggests that imatinib-induced increases in tyrosine phosphorylation of FYN kinase and focal adhesion kinase (FAK) may be responsible for mediating some instances of imatinib resistance and therefore may be potential targets for killing persistent tumor cells and overcoming resistance. The findings also indicate that iTRAQ-based quantitative phosphotyrosine-focused proteomic analysis is a useful way of screening for phosphoproteins associated with drug resistance.

what mechanisms keep these persistent cells alive after shutdown of KIT signaling by imatinib.

Phosphorylation of protein kinases in signaling pathways is a key event in tumor cell survival and proliferation. Differential phosphoprotein analysis may provide clues to alternatively activated pathways and/or substituted kinases that may be activated after inhibition of main pathways, such as KIT.[10] Recent advances in mass spectrometry-based phosphoproteomics enable extensive profiling of serine-threonine kinases, while tyrosine kinase analysis has remained challenging in terms of quantity and quality. However, a recent method coupling peptide-level antiphosphotyrosine immunoaffinity purification with liquid chromatography (LC)-tandem mass spectrometry (MS/MS) has provided reasonable profiling for tyrosine phosphorylation.[11]

In the present study, we quantitatively measured the phosphoproteomic alterations induced by imatinib in a GIST-T1 cell line. We also examined the roles of some tyrosine kinases that were activated in persistent tumor cells after imatinib exposure.

Material and Methods

Cell lines

We previously established the human GIST cell line GIST-T1, which has a 57-nucleotide (V570-Y578) in-frame deletion in KIT exon 11.[12] The cell line identity was confirmed by DNA fingerprinting through short tandem repeat profiling, as previously described.[13] GIST-T1-R was established from GIST-T1 as an imatinib-resistant clone that arose from continuous culturing in 5 μM imatinib. The GIST-T1-R cells GIST-T1-R2 and GIST-T1-R8 each exhibit imatinib IC_{50} values of ~30 μM, which is ~1000 times that of the GIST-T1 parent.

Reagents and antibodies

Imatinib and TAG372—selective tyrosine kinase inhibitors for KIT and focal adhesion kinase (FAK), respectively—were synthesized and provided by Novartis Pharmaceuticals (Basel, Switzerland). The following primary antibodies were used: anti-phospho-Src Family (Tyr416) (1:1000), anti-phospho-ERK and anti-ERK from Cell Signaling Technology (Danvers, MA); anti-GAPDH from Santa Cruz Biotechnology (Santa Cruz, CA); anti-phospho-FAK (Tyr397) from Biosource (Camarillo, CA); anti-FAK from BD Transduction Laboratories (San Jose, CA) and anti-phosphotyrosine (clone 4G10) from Upstate Biotechnology (Lake Placid, NY). Detailed immunoprecipitation information is provided in the Supporting Information Materials and Methods section.

Peptide synthesis

A tyrosine-phosphorylated peptide (NVPLyK) derived from a trypsinized peptide sequence of yeast alpha-enolase was synthesized at Sigma Aldrich (Milwaukee, WI) using standard solid-phase peptide synthesis techniques and Fmoc chemistry.

Phosphopeptide immunoprecipitation

GIST-T1 cells were treated with 400 nM of imatinib for 0, 1, 6 and 24 hr. Tyrosine-phosphorylated peptides were purified using Cell Signaling PhosphoScan pTyr100 Kits (Beverly, MA) following the manufacturer's instructions with minor modification. Detailed information is provided in the Supporting Information Materials and Methods section.

iTRAQ labeling

After immunoprecipitation, peptides were dissolved in 9.8 M Urea (5 μL) and 1 M TEAB (20 μL). Following the manufacturer's protocol (Applied Biosystems, Foster City, CA), the samples were labeled with the isobaric tags for relative and absolute quantitation (iTRAQ) reagents as follows: GIST-T1 with reagent 114 (0 hr), GIST-T1 with reagent 115 (1 hr), GIST-T1 with reagent 116 (6 hr) and GIST-T1 with reagent 117 (24 hr). The labeled peptide samples were then pooled and desalted with Sep-Pak Light C18 Cartridges, and the peptides were dried in a SpeedVac. The labeled peptide mixtures were purified and fractionated into 14 fractions using strong cation exchange fractionation, as previously described.[13]

Quantitative mass spectrometric analysis

Nano LC-MS/MS analysis and iTRAQ data analysis were performed as described in the Supporting Information Materials and Methods section.

Small interfering RNA transfection

Commercial FAK small interfering RNA (siRNA) and nonspecific siRNA were obtained from QIAGEN. Cells were transfected with siRNA using Lipofectamine 2000 reagent (Invitrogen) following the manufacturer's instructions. Selective silencing of FAK was confirmed by western blot analysis.

Generation of FYN knockdown cells

To generate stable FYN knockdown cell lines, GIST-T1 cells were transfected with a commercial plasmid containing an anti-FYN short hairpin RNA (shRNA Fyn, plasmid KH00147N; SABiosciences [Qiagen], Frederick, MD) using Lipofectamine 2000 (Invitrogen, Carlsbad, CA) according to the manufacturer's instructions. The correctly transfected and expressing cells were selected with 600 μg/mL G418 (Invitrogen). Stable clones were maintained in 250 μg/mL G418. Three stable GIST-T1-FYN shRNA cell lines were established, designated B1, B2 and B3 cells. We also established a control cell line of GIST-T1 stably transfected with the empty vector, which we designated GIST-T1-C.

Measurement of IC_{50} after imatinib treatment

Cells were seeded in 96-well plates at 2000 cells/well (Costar; Corning, Corning, NY) for 24 hr and then exposed to various concentrations (0–40 μM) of imatinib for 72 hr. Cell proliferation was evaluated with the WST-8 [2-(2-methoxy-4-nitrophenyl)-3-(4-nitrophenyl)-5-(2,4-disulfophenyl)-2H-tetrazolium, monosodium salt] assay (Cell Counting Kit-SF; Nacalai Tesque) at the indicated post-treatment times. A microplate reader Model 680 (Bio-Rad Laboratories, Hercules, CA) was used to measure WST-8 absorption at a wavelength of 450 nm with a reference wavelength of 630 nm. Growth rate was expressed as the percentage of absorbance for treated cells vs. control cells. Experiments were performed in triplicate in two independent experiments, and the presented values are the averages of all six wells.

Apoptosis assay

GIST-T1 cells were seeded in 6-well plates at a density of 3×10^5 cells per well and treated with imatinib and/or TAG372 for 2 days. The cells were then washed with PBS, and caspase-3 activity was detected using the caspase-3 fluorometric assay kit (R&D systems, Minneapolis, MN) following the manufacturer's instructions. The presented values are the means of three independent experiments.

Statistical analysis

Statistical analyses were performed using the Mann–Whitney *U*-test or one-way analysis of variance (ANOVA), followed by Scheffe's test. One-way ANOVA followed by Dunnett's test was used for multiple comparisons.

Results

Quantitative phosphotyrosine proteomic analysis identifies upregulation of FYN and FAK in imatinib-exposed GIST-T1 cells

GIST-T1 cells that possessed the activating mutation in exon 11 of *KIT* are sensitive to imatinib, with a K_i value for imatinib of 20 nM. Time-dependent decreases in the tyrosine phosphorylation of KIT were observed when GIST-T1 cells were treated with 400 nM imatinib for 0, 1, 6 and 24 hr (Fig. 1*a*). These time-points were used for subsequent MS analysis, with 0 hr used as a control.

By utilizing immunoaffinity enrichment of phosphotyrosine peptides with quantitative phosphoproteomic analysis using iTRAQ technology combined with nano LC-MS/MS analysis, we identified 171 tyrosine phosphorylation sites spanning 134 proteins (Supporting Information Table S1). After imatinib treatment, a total of 11 phosphotyrosine sites spanning 11 proteins exhibited increases of >1.5-fold and 21 phosphotyrosine sites spanning 15 proteins showed decreases of <0.3-fold (Table 1). As a representative protein, we confirmed a dramatic decrease in the tyrosine phosphorylation levels of the KIT protein (Y609, Y703, Y747, Y823 and Y936). In contrast, imatinib induced increased phosphorylation of FYN (Y420) and FAK (Y576). Phosphorylation of FYN (Y420) upregulates tyrosine kinase activities, and phosphorylation of FAK (Y576) is critical for its maximal catalytic activity.

To validate these results obtained from iTRAQ analysis, we further examined the tyrosine phosphorylation of FYN and FAK using western blotting. As shown in iTRAQ analysis, western blotting confirmed that FYN (Y420) and FAK (Y576) were time dependently phosphorylated (Figs. 1*b* and 2*c*). When tyrosine phosphorylation in the activation loop was measured for other Src family kinases, we found that imatinib treatment did not increase tyrosine phosphorylation of SRC, LYN, LCK or YES (Fig. 1*b*).

Inhibition of FYN or FAK enhances imatinib sensitivity of GIST-T1 cells

To examine the functions of FYN in GIST-T1 cells exposed to imatinib, FYN expression was stably suppressed using a FYN shRNA plasmid. We cloned and established GIST-T1 B1, B2 and B3 cells, as well as GIST-T1 C cells transfected with empty vector as a control (Fig. 1*d*). Compared with GIST-T1 C cells, the FYN knockdown cell lines showed significantly decreased IC_{50} values for imatinib ($p < 0.05$; Fig. 1*d*).

We also examined the role of FAK activation in imatinib treatment. We repressed FAK expression using siRNA, and we used a FAK inhibitor (TAG372) to inhibit FAK phosphorylation. Transfection of FAK siRNA reduced IC_{50} values for imatinib ($p < 0.05$; Fig. 1*e*). When used with imatinib, TAG372 further decreased cell survival in a dose-dependent manner (Fig. 1*f*).

Inhibition of FAK improves imatinib sensitivity in GIST-T1-R cells

Next, we examined FAK activation in imatinib-resistant cell lines established from GIST-T1 cells. Eight imatinib-resistant cell lines were established by incubation of GIST-T1 cells with imatinib of gradually increased concentrations. Constitutive phosphorylation of FAK was observed in two imatinib-resistant

Short Report

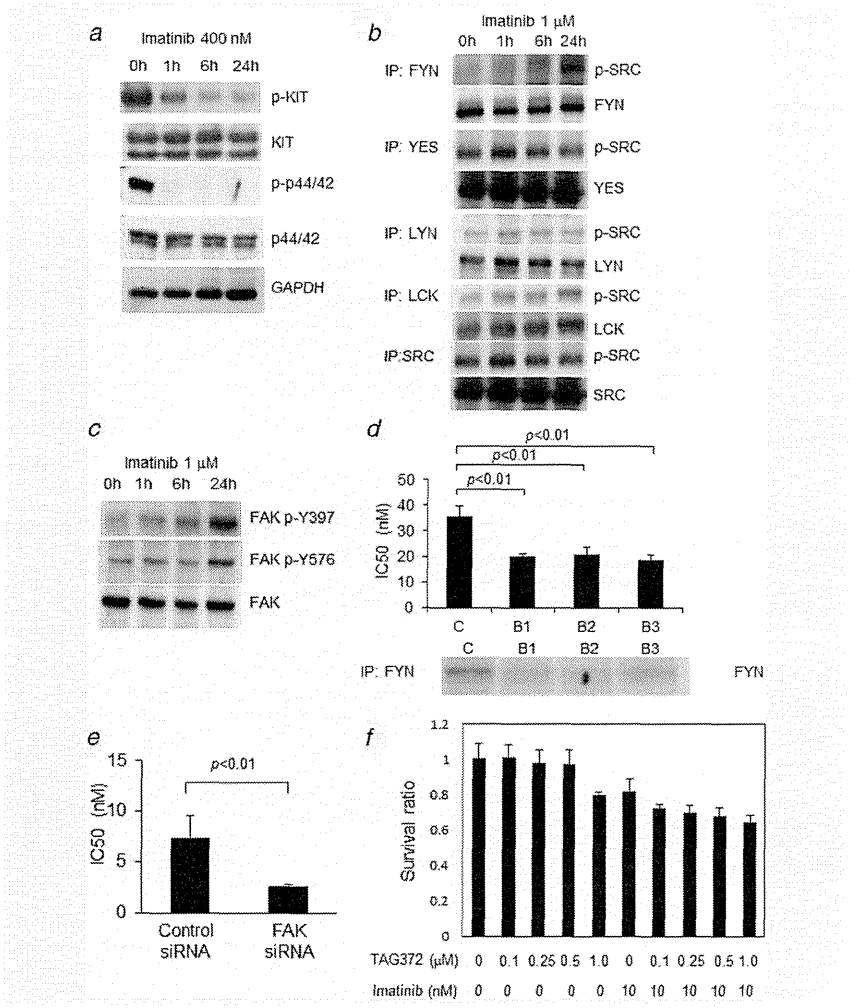

Figure 1. (*a*) Altered tyrosine phosphorylation levels detected by iTRAQ analysis were confirmed by western blotting. Imatinib treatment led to reduced phosphotyrosine levels. (*b*) Imatinib treatment changed SRC family kinase phosphorylation levels. (*c*) iTRAQ analysis showed that FYN (Y420) and FAK (Y576) exhibited similar tyrosine phosphorylation. (*d*) Compared with in GIST-T1 C cells, the IC_{50} for imatinib was significantly reduced in all FYN knockdown GIST-T1 cells (B1, B2 and B3). (*e*) The IC_{50} for imatinib was reduced in GIST-T1 cells that were transfected with FAK siRNA. (*f*) WST-8 assay showed the cell viability with imatinib and TAG372 treatment. Data are presented as means ± SD.

Table 1. Phosphotyrosine peptides that were increased or decreased by imatinib treatment, as quantified by iTRAQ analysis[1]

Accession Number	Sequence	Description	Site	1 hr/0 hr[2]	6 hr/0 hr[2]	24 hr/0 hr[2]
Greater than 1.5-fold increase of phosphorylated peptide at 24 hr compared with 0 hr						
P06241	LIEDNEYTAR	Tyrosine-protein kinase Fyn	Y420	0.845	2.365	3.641
P15880	AFVAIGDYNGHVGLGVK	40S ribosomal protein S2	Y133	2.138	1.807	2.443
O00401	VIYDFIEK	Neural Wiskott-Aldrich syndrome protein	Y256	0.768	1.491	1.978
Q99623	MLGEALSKNPGYIK	Prohibitin-2	Y248	1.446	1.778	1.726
P62829	NLYIISVK	60S ribosomal protein L23	Y38	2.138	1.348	1.679
P18433	VVQEYIDAFSDYANFK	Receptor-type tyrosine-protein phosphatase alpha	Y791	1.245	1.098	1.667
P30040	FDTQYPYGEK	Endoplasmic reticulum resident protein 29	Y64	1.804	2.558	1.640
Q05397	YMEDSTYYK	Focal adhesion kinase 1	Y570	1.043	0.893	1.606
A6NI28	LDTASSNGYQRPGSVVAAK	Rho GTPase-activating protein 42	Y792	0.599	0.980	1.594
P08758	LYDAYELK	Annexin A5	Y94	1.043	1.399	1.581
P18669	HYGGLTGLNK	Phosphoglycerate mutase 1	Y92	0.930	2.583	1.532
Less than 0.3-fold reduction of phosphorylated peptide at 24 hr compared with 0 hr						
P10721	IGSYIER	Mast/stem cell growth factor receptor Kit	Y747	0.649	0.244	0.291
O95490	SENEDIYYK	Latrophilin-2	Y1350	0.431	0.318	0.256
Q92569	LQEYHSQYQEK	Phosphatidylinositol 3-kinase regulatory subunit gamma	Y184	0.433	0.271	0.255
P10721	QEDHAEAALYK	Mast/stem cell growth factor receptor Kit	Y703	0.560	0.207	0.254
P10721	QISESTNHIYSNLANCSPNR	Mast/stem cell growth factor receptor Kit	Y936	0.445	0.212	0.244
Q92796	RDNEVDGQDYHFVVSR	Disks large homolog 3	Y673	0.556	0.427	0.241
Q5XXA6	STIVYEILKR	Anoctamin-1	Y251	0.508	0.720	0.235
Q00535	IGEGTYGTVFK	Cyclin-dependent kinase 5	Y15	1.877	0.821	0.232
Q06481	MQNHGYENPTYK	Amyloid-like protein 2	Y755	0.474	–[4]	0.220
O95297	INKSESVVYADIR	Myelin protein zero-like protein 1	Y263	0.785	0.249	0.211
Q969M3	QYAGYDYSQQGR	Protein YIPF5	Y42	0.145	–[4]	0.195
O14964	VVQDTYQIMK	Hepatocyte growth factor-regulated tyrosine kinase substrate	Y132	1.097	0.464	0.173
O95297	SESVVYADIR	Myelin protein zero-like protein 1	Y263	0.563	0.169	0.166
Q92569	VQAEDLLYGKPDGAFLIR	Phosphatidylinositol 3-kinase regulatory subunit gamma	Y373	1.186	0.176	0.130
O96000	YQDLGAYSSAR	NADH dehydrogenase [ubiquinone] 1 beta subcomplex subunit 10	Y143	0.864	0.393	0.122
P16333	LYDLNMPAYVK	Cytoplasmic protein NCK1	Y112	0.651	0.257	0.103
Q12846	NILSSADYVER	Syntaxin-4	Y251	0.179	0.131	0.072
Q8N128	YQYAIDEYYR	Protein FAM177A1	Y162	0.196	0.090	0.055
P10721	VVEATAYGLIK	Mast/stem cell growth factor receptor Kit	Y609	0.723	–[4]	0.023
P10721	DIKNDSNYVVK	Mast/stem cell growth factor receptor Kit	Y823	0.164	–[4]	–[4]
P53778	QADSEMTGYVVTR	Mitogen-activated protein kinase 12	Y185	1.582	0.888	–[4]

[1]The full list is provided in Supporting Information Table 1.
[2]The ratio of peptide derived from the iTRAQ reporter ion, as determined by iTRAQ analysis; 1 hr/0 hr, 6 hr/0 hr and 24 hr/0 hr refer, respectively, to the value of each peptide at 1, 6 and 24 hr divided by the value of that peptide at 0 hr.
[3]A 0-hr value of 0 (*i.e.* below background) and a positive value at 1, 6 or 24 hr.
[4]A 0-hr positive value and a value of 0 (*i.e.* below background) at 1, 6 or 24 hr.

Short Report

GIST-T1 cell lines (GIST-T1-R2 and GIST-T1-R8), which had imatinib IC_{50} values of 30 μM, ~1000 times that of the GIST-T1 parent cells (Fig. 2*a*). TAG372 dose dependently inhibited FAK phosphorylation in GIST-T1-R2 (Fig. 2*b*), and significantly reduced the imatinib IC_{50} values when both drugs were used (Fig. 2*c*). Moreover, TAG372 induced apoptosis in GIST-T1-R2 (Fig. 2*d*). These results indicate that imatinib treatment induced activation of FYN and FAK in persistent GIST-T1 cells and was associated with imatinib insensitivity and resistance.

Discussion

Imatinib is a selective tyrosine kinase inhibitor of KIT, PDGFRA, ABL/BCR-ABL and CSF-1R, which was first used to treat GIST in 2000. Since then, it has been a standard treatment for advanced and/or recurrent GISTs.[6] Patients with advanced GIST usually respond to imatinib; however, most patients eventually experience disease progression with the reactivation of KIT tyrosine kinase and its downstream signaling pathways.[14,15] Although imatinib has high activity against GISTs, it cannot achieve complete eradication of tumor cells *in vivo* or *in vitro*. Results of the BFR14 trial showed that stopping imatinib treatment, even after complete response, resulted in disease progression or recurrence.[7,8] In chronic myelogenous leukemia (CML), mathematical models have indicated that secondary mutations might emerge after imatinib therapy;[16] therefore, residual tumor cells may also be a predisposing factor for acquired resistance to imatinib in GIST.

To quantitate the alteration of tyrosine phosphorylation levels induced by imatinib, we established quantitative tyrosine phosphoproteomic analysis. Using this technology, we identified 171 different tyrosine phosphorylation sites in 134 proteins of GIST-T1 cells. As we were searching for alternative pathways that were activated after inhibition of KIT signaling by imatinib, we pursued tyrosine kinases with increased tyrosine phosphorylation. Our comprehensive measures indicated that 11 tyrosine kinases exhibited tyrosine phosphorylation increases of greater than 1.5-fold (Table 1). The findings of the phosphoproteomic analysis were confirmed by western blotting showing the tyrosine-phosphorylation of KIT, FAK and other src-family kinases. SRC and LYN are reportedly phosphorylated and activated in GIST after imatinib treatment;[18] however, in the phosphoproteomic and western blotting analyses in the present study, we did not detect activation of SRC, LYN, YES, Lck or any other Src family kinases, except for FYN and FAK. Activation of FYN and FAK is reportedly involved in tumor proliferation and malignant transformation.[17–20]

FYN appears to participate in cell growth and survival, acting downstream of integrin and PI3K.[17,21] Although the shRNA silencing of FYN induced additional cell death in GIST-T1 cells during imatinib treatment, dasatinib (a SRC family kinase inhibitor) had no effect in combination with imatinib (data not shown). These results suggest the involvement of FYN in alternative survival signaling pathways.

FAK is also a nonreceptor tyrosine kinase that is activated through autophosphorylation at Tyr^{397} by integrin and growth factor receptors; this is followed by subsequent activation of other functional phosphorylation sites to transduce the signals to downstream pathways.[22,23] FAK is reportedly overexpressed in malignant GISTs and correlated with recurrence.[19] Furthermore, FAK phosphorylation is associated with imatinib-resistance of a KIT exon 17 mutation, but not exon 11 mutation.[20] This imatinib-resistance was diminished by TAE226, which inhibits FAK and insulin-like growth factor-1 receptor. Our findings showed that imatinib induced time-dependent FAK activation in GIST-T1 cells with an imatinib-sensitive mutation of KIT exon 11. Moreover, FAK inhibition using either a FAK-specific TAG372 inhibitor or siRNA decreased the viability of GIST-T1 cells under imatinib treatment. TAG372 also induced apoptosis in imatinib-resistant cell lines with FAK activation. Taken together, it appears that FAK activation may be a critical survival signal of GIST cells under imatinib treatment, and targeting FAK with imatinib may be a promising therapeutic approach.

When imatinib was removed, KIT was quickly rephosphorylated, and FYN and FAK were simultaneously dephosphorylated (data not shown), suggesting that alternative pathway activation is functional during imatinib treatment, and may not be accompanied with qualitative changes, such as new mutations. FYN inhibition was accompanied with a subsequent lack of FAK activation, while FAK inhibition resulted in increased FYN phosphorylation, thus indicating that FYN acted upstream of FAK. However, the critical changes that induce FYN activation and subsequent FAK phosphorylation remain unknown. Additional studies are required to elucidate the FYN activation mechanisms and the alternative pathways induced by imatinib, as well as their association with acquired drug resistance.

In summary, here we found that imatinib induced increased tyrosine phosphorylation of FYN and FAK in GIST-T1 cells. Blockade of these tyrosine kinases might be a potential target to overcome imatinib resistance. Additionally, iTRAQ-based quantitative phosphotyrosine-focused proteomic analysis appears to be a useful approach to screening for phosphoproteins associated with drug resistance.

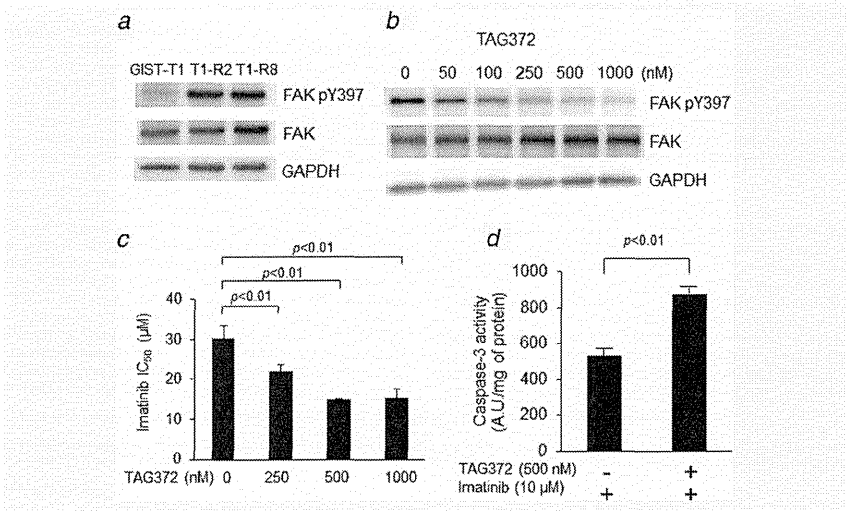

Figure 2. (*a*) Constitutive phosphorylation of FAK was observed in GIST-T1-R cells (GIST-T1-R2 and GIST-T1-R8). (*b*) Constitutive phosphorylation of FAK was observed in imatinib-resistant GIST-T1 cells (GIST-T1-R2), and TAG372 dose dependently inhibited this phosphorylation. (*c*) TAG372 reduced the IC_{50} of imatinib and induced apoptosis in GIST-T1-R2 cells. (*d*) TAG372 induced apoptosis in GIST-T1-R2 cells. Data are presented as means ± SD.

Acknowledgments

This study was partly supported by grants from Novartis Pharmaceuticals.
Conflict of interest: N.T. has honoraria to disclose from the Novatis, Pfizer and Bayer within past 2 years.

References

1. Hirota S, Isozaki K, Moriyama Y, et al. Gain-of-function mutations of c-kit in human gastrointestinal stromal tumors. *Science* 1998;279:577–80.
2. Nishida T, Hirota S, Taniguchi M, et al. Familial gastrointestinal stromal tumours with germline mutation of the kit gene. *Nat Genet* 1998;19:323–4.
3. Hirota S, Ohashi A, Nishida T, et al. Gain-of-function mutation of platelet-derived growth factor receptor αgene in gastrtointestinal stromal tumors. *Gastroenterology* 2003;125:660–7.
4. Verweij J, Casali PG, Zalcberg J, et al. Progression-free survival in gastrointestinal stromal tumours with high-dose imatinib: randomised trial. *Lancet* 2004;364:1127–34.
5. Blanke CD, Rankin C, Demetri GD, et al. Phase III randomized, intergroup trial assessing imatinib mesylate at two dose levels in patients with unresectable or metastatic gastrointestinal stromal tumors expressing the kit receptor tyrosine kinase: S0033. *J Clin Oncol* 2008;26:626–32.
6. Demetri GD, von Mehren M, Blanke CD, et al. Efficacy and safety of imatinib mesylate in advanced gastrointestinal stromal tumors. *N Engl J Med* 2002;347:472–80.
7. Blay JY, Le Cesne A, Ray-Coquard I, et al. Prospective multicentric randomized phase III study of imatinib in patients with advanced gastrointestinal stromal tumors comparing interruption versus continuation of treatment beyond 1 year: the French Sarcoma Group. *J Clin Oncol* 2007;25:1107–13.
8. Le Cesne A, Ray-Coquard I, Bui BN, et al. Discontinuation of imatinib in patients with advanced gastrointestinal stromal tumours after 3 years of treatment: an open-label multicentre randomised phase 3 trial. *Lancet Oncol* 2010;11:942–9.
9. Nishida T, Shirao K, Sawaki A, et al. Efficacy and safety profile of imatinib mesylate (ST1571) in Japanese patients with advanced gastrointestinal stromal tumors: a phase II study (ST1571B1202). *Int J Clin Oncol* 2008;13:244–51.
10. Mann M, Ong SE, Grønborg M, et al. Analysis of protein phosphorylation using mass spectrometry: deciphering the phosphoproteome. *Trends Biotechnol* 2002;20:261–8.
11. Rush J, Moritz A, Lee KA, et al. Immunoaffinity profiling of tyrosine phosphorylation in cancer cells. *Nat Biotechnol* 2005;23:94–101.
12. Taguchi T, Sonobe H, Toyonaga S, et al. Conventional and molecular cytogenetic characterization of a new human cell line, GIST-T1, established from gastrointestinal stromal tumor. *Lab Invest* 2002;82:663–5.
13. Yokoyama T, Enomoto T, Serada S, et al. Plasma membrane proteomics identifies bone marrow stromal antigen 2 as a potential therapeutic target in endometrial cancer. *Int J Cancer* 2013;132:472–84.
14. Nishida T, Kanda T, Nishitani A, et al. Secondary mutations in the kinase domain of the KIT gene are predominant in imatinib-resistant gastrointestinal stromal tumor. *Cancer Sci* 2008;99:799–804.
15. Antonescu CR, Besmer P, Guo T, et al. Acquired resistance to imatinib in gastrointestinal stromal tumor occurs through secondary gene mutation. *Clin Cancer Res* 2005;11:4182–90.
16. Michor F, Hughes TP, Iwasa Y, et al. Dynamics of chronic myeloid leukaemia. *Nature* 2005;435:1267–70.
17. Timokhina I, Kissel H, Stella G, et al. Kit signaling through PI 3-kinase and Src kinase pathways: an essential role for Rac1 and JNK activation in mast cell proliferation. *EMBO J* 1998;17:6250–62.
18. Rossi F, Yozgat Y, de Stanchina E, et al. Imatinib upregulates compensatory integrin signaling in a mouse model of gastrointestinal stromal tumor and is more effective when combined with dasatinib. *Mol Cancer Res* 2010;8:1271–83.
19. Koon N, Schneider-Stock R, Sarlomo-Rikala M, et al. Molecular targets for tumour progression in gastrointestinal stromal tumours. *Gut* 2004;53:235–40.
20. Sakurama K, Noma K, Takaoka M, et al. Inhibition of focal adhesion kinase as a potential therapeutic strategy for imatinib-resistant gastrointestinal stromal tumor. *Mol Cancer Ther* 2009;8:127–34.
21. Linnekin D, DeBerry CS, Mou S. Lyn associates with the juxtamembrane region of c-Kit and is activated by stem cell factor in hematopoietic cell lines and normal progenitor cells. *J Biol Chem* 1997;272:2745–55.
22. Serrels A, McLeod K, Canel M, et al. The role of focal adhesion kinase catalytic activity on the proliferation and migration of squamous cell carcinoma cells. *Int J Cancer* 2012;131:287–97.
23. Cox BD, Natarajan M, Stettner MR, et al. New concepts regarding focal adhesion kinase promotion of cell migration and proliferation. *J Cell Biochem* 2006;99:35–52.